A level set approach to simulate grain growth with an evolving population of second phase particles

Karen Alvarado[1], Sebastian Florez[1], Baptiste Flipon[1], Nathalie Bozzolo[1], Marc Bernacki[1]

[1] Mines-ParisTech, PSL-Research University, CEMEF - Centre de mise en forme des matériaux, CNRS UMR 7635, CS 10207 rue Claude Daunesse, 06904 Sophia Antipolis Cedex, France

E-mail: karen.alvarado@mines-paristech.fr

2 December 2020

Abstract. In numerous polycrystalline materials, grain size is controlled by second phase particles (SPPs) that hinder the grain boundaries (GBs) by pinning mechanisms. The Smith-Zener pinning (SZP) model describes the physical interaction between SPPs and GBs. Both of them can evolve when applying a heat treatment to the material. As industrial forging processes involve hot deformation steps near the solvus temperature, it is thus of prime importance to characterize the evolution of the SPPs due to their impact on the final microstructure, notably on the grain size.

The level set (LS) method is classically used to describe the influence of SPPs on grain growth (GG) by considering the simulated particles as inert and represented by static holes in the used finite element (FE) mesh. A new formalism to model GG mechanism under the influence of the SZP phenomenon, able to take into account evolving particles is proposed. It involves the representation of SPPs by a LS function and a particular numerical treatment around the grain interfaces encountering SPP, making possible the modelling of SPPs evolution without altering the undergoing pinning pressure. Validation and comparison of the new method regarding previous FE-LS formulation in 2D and 3D simulations and an application on GG under the influence of dissolving particles are described.

Submitted to: *Modelling Simul. Mater. Sci. Eng.*

1. Introduction

The SZP describes the interaction between particles and GBs [1]. For materials like the γ/γ' superalloys that present a matrix phase (γ) and a particle phase (γ'), GG can be hindered by the γ' phase, enabling to control the mean grain size of the microstructure during the forming processes of these materials. This is also presented in other materials like steels, for instance where the particles facilitate the grain refinement [2, 3]. The described phenomenon was first discussed by Smith [1] and then detailed by Zener one year after [4]. Since these first developments to equate this phenomenon, many variants have been developed in order to dispel some of the initial hypotheses (see [5, 6, 7, 8]).

In the context of GG, the classical Smith-Zener equation relates the average radius of grains $\overline{R}$ of a given stable microstructure with the average radius $\overline{r}$ of precipitates and their volume fraction f. This equation provides the stationary mean grain radius based on the balance of driving pressures.

Nowadays, it is well known that the original equation overestimates the limit grain size due to an overestimation of the capillarity driving pressure P_G or an underestimation of the pinning pressure P_Z which both rely on numerous hypotheses. In fact, these pressures depend on several factors like particle morphology, particle/matrix interaction (coherency), grain and particle size distributions...

Finally, the Smith-Zener equation can be generalized as:

$$\overline{R} = K\frac{\overline{r}}{f^m}, \tag{1}$$

where K and m are fitted parameters which can be assumed constant, nonetheless these values vary depending on the authors and the assumptions made to obtain P_Z [5, 7, 8, 9]. Some of them consider only the particles located at the GBs, because only these particles act on the GBs.

Due to the importance of predicting the properties of the materials, this phenomenon has been largely studied thanks to full field numerical methods at the polycrystalline scale.

One can cite probabilistic techniques such as Monte Carlo (MC) [7, 10, 11, 12, 13, 14] and Cellular Automata (CA) [15, 16] methods where SPPs are described thanks to voxels/cells with a specific orientation. These sites are not allowed to be reoriented, so particles are assumed immobile and the real interactions between SPPs and GBs are roughly taken into account. For small SPPs (comparatively to the voxel size), some variants exist where an equivalent pinning pressure is introduced for voxels containing SPPs [17, 18]. Front-tracking models such as vertex methodologies [19], where the grains boundaries are simulated by linear segments, are also used. In these approaches, the SPPs are described as "pinning centers" where the pinning pressure must be overcame to liberate pinning GBs. Thus, while these approaches are effective and enable an accurate calculation of grain boundary curvature, they limit drastically the description of the SPPs (shape, evolution, size).

Recently, the use of front-capturing methods like the phase-field (PF) [9, 20, 21, 22,

23, 24, 25, 26, 27] and level-set (LS) [28, 29, 30, 31, 32, 33, 34] have been developed to describe grain interfaces thanks to implicit mathematical functions. In the PF model, the particles are usually represented by adding a new space-dependent energy term in the total free energy system and complex shape [26] or properties [24] of SPPs can also be considered. In the LS approach, they are described as holes in the domain where Neumann boundary conditions are imposed to the LS functions in order to respect the Young-Herring equilibrium in the contact positions between GBs and SPPs.

To our knowledge, the simulation of GG in presence of SSPs based on the LS method has initially be proposed by Agnoli et al. [28], further studied and improved by Scholtes et al. [29] in a 3D context. In their model, it is possible to introduce a spherical population of SPPs and also to generate particles with a real morphology extracted from Electron backscatter diffraction (EBSD) maps or secondary electron (SE) images. However, this approach has some limitations mainly because the SPPs are described with static holes and refined FE meshes at their interfaces are required:

- the simulation of material deformations seems not straightforward when one wants to take into account the SPP behaviour as the SPPs are not described in volume in the considered FE mesh,
- the previous remark could be crucial when dynamic recrystallization is investigated. Indeed, it is well-known that the SPPs interfaces are favorable sites for the appearance of new grains. Thus, a fine description of the mechanical fields at the SPPs interfaces is necessary but impossible, at yet, in the existing LS formulations,
- the simulation time can be drastically increased by the remeshing operations around the particles and the GBs, mainly in 3D,
- the evolution of SPPs, due to diffusive mechanisms, such as precipitation/dissolution, Ostwald ripening, agglomeration, spheroidization can not be taken into account (as SPPs are considered static in the existing LS formulations).

For these reasons, a new LS approach to model GG mechanisms in presence of meshed SPPs and able to reproduce evolving particles is proposed. In this work, the description of SPPs is made by a new level set function over the domain calculation without considering holes in the FE mesh. A numerical treatment around the grain interfaces surrounding the SPPs, that ensures a good description of the pinning pressure and makes it possible to migrate the SPPs interface has been developed. At the same time, the new formalism opens the possibility to simulate material deformations more naturally by taken into account the mechanical behavior of SPPs. Validation and comparisons of the proposed numerical framework comparatively to previous formulations [28, 29] followed by the GG simulations of a representative nickel base superalloy microstructure are presented.

2. Interface treatment

2.1. Level-set modelling of polycrystals

The full field simulations presented in this work are based on the level set (LS) method in a P1 FE framework. This method enables the calculation of the position of an interface $\Gamma(t) = \partial G$ governed by a velocity field $\overrightarrow{v}$. The interface is represented as the interpolated zero-isovalue of a function $\varphi(x,t)$ classically, defined as the Euclidean distance to the interface [35]:

$$\begin{cases} \varphi(x,t) = \pm d\left(x, \Gamma(t)\right), x \in \Omega \\ \Gamma(t) = \{x \in \Omega, \varphi(x,t) = 0\} \end{cases} \tag{2}$$

where $d\left(x, \Gamma(t)\right)$ is the Euclidean distance between a point x and the boundary $\Gamma(t)$ of the considered object G and Ω the calculation domain. When the interior of G is not the empty set, such as for grains in polycrystals, the sign convention is often adopted as φ positive inside and negative outside. Hence, the interface migration can be deduced by the resolution of a convection equation:

$$\frac{\partial \varphi}{\partial t} + \vec{v} \cdot \nabla \varphi = 0. \tag{3}$$

When GG phenomenon is considered, the minimization of the system energy is piloted by the mean curvature flow (minimization of the interface energy), so, the grain boundaries velocity can be approximated by the following relationship:

$$\vec{v} = -M\gamma\kappa\vec{n}, \tag{4}$$

where M is the mobility of the grain interface, γ the grain boundary energy, $\kappa = \nabla \cdot \vec{n}$ the local mean curvature (i.e. the curvature in 2D and the sum of the main curvatures in 3D) and $\vec{n} = -\frac{\nabla\varphi}{|\nabla\varphi|}$ the outward unitary normal vector to the interface. It must be highlighted that if the kinetics framework of Eq.(3) is often used with the classical assumption of an Arrhenius law for the description of the mobility (temperature dependence) and a homogeneous description of γ [32] as considered in the following of this article, it can be extended to more complex configurations with a heterogeneous description of γ (dependence to the misorientation angle) [36, 37, 38], anisotropic description of γ (dependence to the inclination of the grain boundaries) [39] and richer description of M (dependence to the misorientation or solute aspect) [40].

Theoretically, each grain of a polycrystal must be represented by its own LS function. In order to reduce the computation time and memory storage, several non-neighboring grains in the initial microstructure (separated by a certain number of grains) can be grouped to form Global Level Set (GLS) functions thanks to Graph coloration technique. However, the grains belonging to the same function can no longer be distinguished. As a consequence, when two child grains of a GLS grow and meet each other, numerical coalescence occurs, i.e. both grains merge to form a single one. Thus different strategies can be found to avoid these numerical coalescence events. Here,

a re-coloration algorithm, developed by Scholtes et al. [29, 41], will be considered at each time step. The number of GLS functions, N is then always drastically reduced compared to the number of grains N_G. This method is efficient in terms of memory and performance, allowing LS-FE simulations with a large number of grains even for 3D simulations [33]. In the following, the index i will denote the set of GLS used to describe the entire polycrystal.

Assuming that $|\nabla\varphi_i| = 1$, $\forall i \in [\![1, N]\!]$, i.e. φ_i remain distance functions all along the simulation, Eq.(3) can be reformulated as a set of diffusive equations meaning that the calculations of the curvatures and the normal vectors at grain interfaces are no longer required.

$$\begin{cases} \frac{\partial\varphi_i}{\partial t} - M\gamma\Delta\varphi_i = 0 \\ \varphi_i(t=0,x) = \varphi_i^0 \quad \forall i \in [\![1, N]\!] \end{cases} \tag{5}$$

where φ_i^0 is the initial distance function of each GLS. A major drawback of the LS formulation lies in the fact that, after the resolution of Eq.(5), the GLS are no longer distance functions $|\nabla\varphi| \neq 1$. This is particularly problematic when a specific remeshing technique depending on the distance property is used at the interface. In addition, the diffusive formulation proposed in Eq.(5) requires a distance function at least in a thin layer around the interface in order to properly compute the mean curvature flow mechanism. Finally, the conditioning of the transport problem also depends on the regularity of the LS function. For these reasons, the GLS functions need to be reinitialized in order to restore their metric property at each time step. Numerous approaches exist to solve this reinitialization procedure in regular grids or unstructured FE meshes [42, 43, 44]. Here, a recent direct fast and accurate approach usable in unstructured FE mesh proposed by Shakoor et al. is used [45]. Discussions concerning the residual errors inherent to this approach are also discussed in [34].

The presence of non-physical vacuum regions at the multiple junctions, due to the front-capturing description of the grains and following the resolution of Eq.(5) is well known and the following classic procedure, proposed in [30], is used to treat it:

$$\hat{\varphi}_i = \frac{1}{2}\left(\varphi_i - \max_{j\neq i}\varphi_j\right), \quad \forall i = 1\dots N, \tag{6}$$

where $\hat{\varphi}_i$ is then used as the corrected GLS function.

2.2. Particle grain boundary interaction

In previous FE-LS studies [28, 29] where the particles were represented as static holes in the domain, no assumption was needed to simulate the pinning effect generated by the particles. Indeed, the SZP effect generated by the presence of particles can be naturally taken into account by imposing the relevant boundary conditions related to the phenomenon at the interfaces between GBs and SPPs. More precisely, the influence of SPP on microstructure evolution can be taken into account by imposing a Neumann

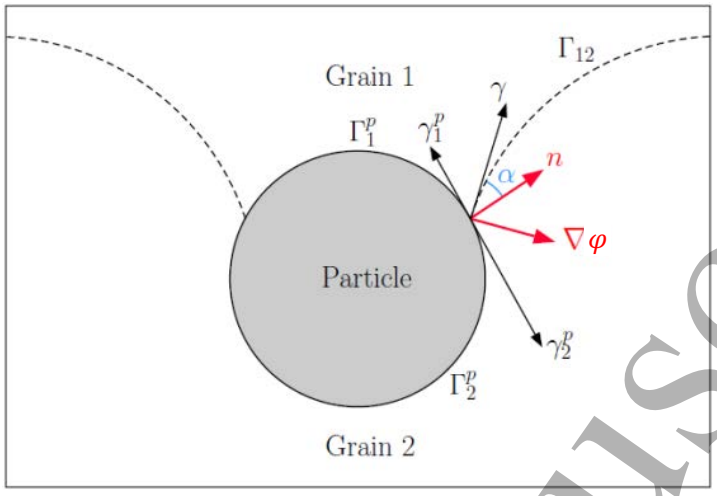

Figure 1: Illustration of the interaction between a particle and a GB (dashed lines between Grain 1 and Grain 2). $\vec{n}$ corresponds to the normal to the particle interface, $\nabla\varphi$ to the normal to the GB and α to the angle established by the balance of surface tensions.

type limit condition on the GLS at the surface of the precipitates following the Young-Herring surface tension equilibrium:

$$\frac{\nabla\varphi}{|\nabla\varphi|}\cdot\vec{n} = \nabla\varphi\cdot\vec{n} = sin(\alpha) = \frac{\gamma_p^2 - \gamma_p^1}{\gamma}, \tag{7}$$

where, as illustrated in Figure 1, $\vec{n}$ is the external unitary normal vector to the precipitate, α is the angle established by the balance of surface tensions at contact positions between the SPP and the grain boundary. So, when the particle is assumed incoherent with the matrix (quite common for superalloys materials [46, 47]), $\gamma_p^1 \simeq \gamma_p^2$, which leads to $\alpha \simeq 0$, a null Neumann boundary condition is applied at the precipitate/grain boundary interface through the respect of Eq.(7).

In our new formalism, where the particles are represented by one new LS function, φ_{SPP}, the GLS fields describing the grains are initially modified with simple topological operations (following by a reinitialization step) to introduce the presence of the SPPs, without modifying the particle interface:

$$\forall i \in [\![1, N]\!] \quad \hat{\varphi}_i\left(t=0,x\right) = min\left(\varphi_i\left(t=0,x\right), -\varphi_{SPP}\left(t=0,x\right)\right). \tag{8}$$

This operation is followed by a reinitialization procedure as the resulting level-set functions are not (when the intersection is not empty) a distance function, even if GLS and φ_{SPP} are. Of course, the function $\varphi_{SPP}\left(t=0,x\right)$ can be easily estimated as the distance function to the union of simple objects (as circles for spherical particles) but also obtained through the FE-immersion of an experimental map [28, 29].

See Figure 2, for an illustration of the resulting modification for two neighbouring GLS.

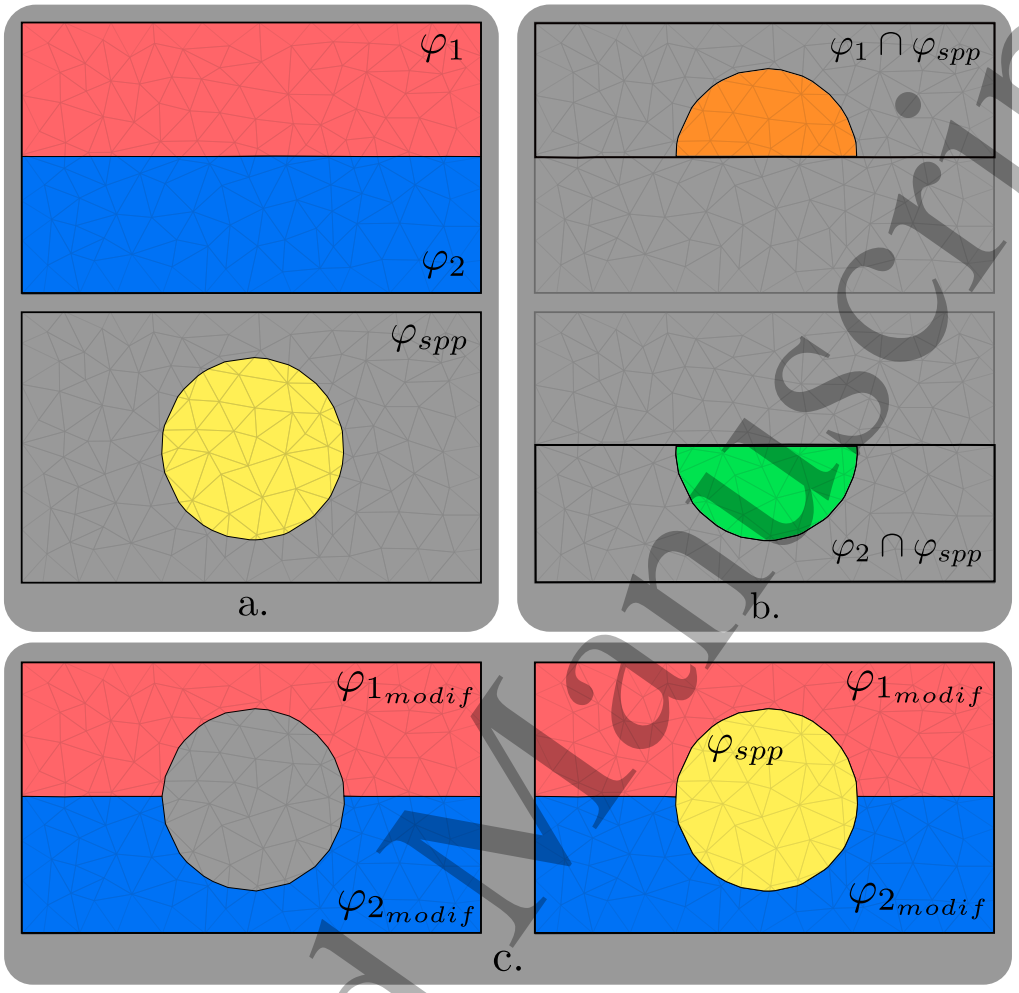

Figure 2: General procedure to modify the GLS functions, only the positive side of the GLS fields is represented by a given color: a) Initial GLS fields of two neighbouring grains (red and blue respectively) and one particle (*yellow*), b) Intersections of grains and SPP fields, c) modification of the GLS, the particle LS φ_{SPP} do not change in the process.

2.3. SPP treatment

As already discussed (see Eq.(6)), the appearance of voids or overlaps especially at the multiple junctions after solving the convective-diffusive equations was first treated by [30] and implement in several cases, in 2D and 3D, using the LS method [29, 32, 33].

In order to respect the Young-Herring equilibrium without hollowing out the SPPs, we propose, at each time step, to simply extend this treatment by taken into account φ_{SPP} in the procedure:

$$\hat{\varphi}_i(t,x) = \frac{1}{2}\left(\varphi_i(t,x) - \max\left(\max_{j\neq i}\left(\varphi_j(t,x)\right), \varphi_{SPP}(t,x)\right)\right), \quad \forall i = 1\ldots N, \quad \forall x \in \Omega. \tag{9}$$

Hereafter, we will call this as the Modified Multiple Junctions Treatment (MMJT). As it will be illustrated in the following, in the zones without SPPs, MMJT is equivalent

to the classical numerical treatment (Eq.(6)) whereas when SPPs are present, it enables, by successive iterations, to impose the Young-Herring equilibrium for incoherent SPPs.

In Figure 3, the GG evolution of one grain (green part denoted by φ_1) in the presence of one spherical particle (yellow part denoted by φ_{spp}) is represented to see the effect of the MMJT. Typical FE mesh size and time step are chosen following classical strategy in the context of FE-LS modelling of GG [48, 49]. When the diffusive equation (Eq.(5)) is solved on φ_1, the grain overlaps the particle LS φ_{spp} (see Figure 3.b). Thus, it is necessary to apply the MMJT (see Figure 3.c).

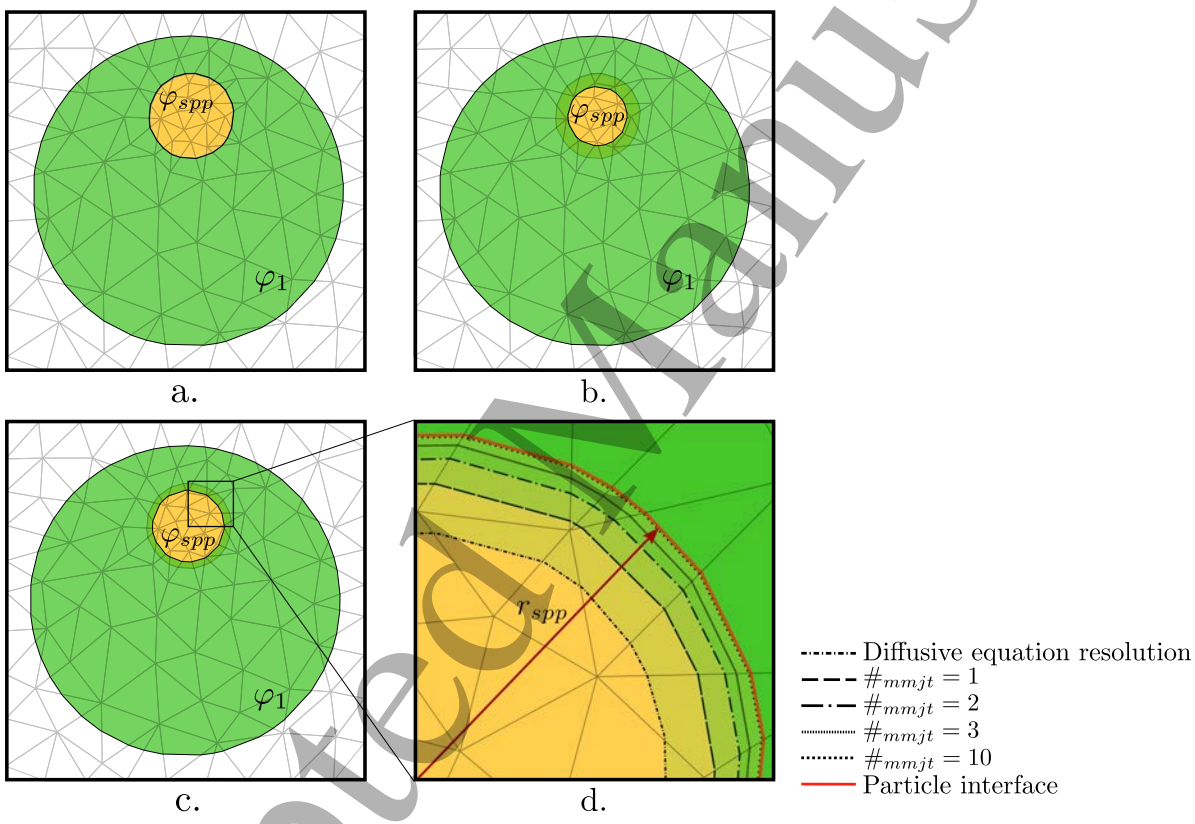

Figure 3: Grain growth evolution of one grain in presence of one SPP represented as an LS and the effects presented on the interfaces. a) Initial LS field of one grain (φ_1) and one particle (φ_{spp}), b) Resolution of the diffusive equation, the grain shrinks due to the curvature flow but also overlaps the particle field, c) The modified multiple junctions treatment (MMJT) is applied one time to correct the overlap, d) The MMJT is applied 1, 2, 3 and 10 times to well describe the initial particle/grain interface.

However, it is clear that after applying Eq.(9) to φ_1, the SPPs/grain interface is not properly defined. In fact, the LS describing the grains have only moved half of the necessary distance to correct the non-physical overlap. This problem can be corrected by the use of multiple consecutive calls of Eq.(9) by keeping φ_{spp} unchanged, these calls reduce each time by a factor 2 the overlapped region between the SPP and the grain interfaces. Hereafter, we will denote by $\#_{mmjt}$ the number of calls of the MMJT.

Now, the remaining question is how many times do we need to call Eq.(9) to reproduce the grain/particle interface correctly? Figure 4 illustrates the previous example with a precipitate of diameter ($D_{spp} = 10\mu m$). As the error is described by a geometric series when not multiples joints are present (only one interface particle/grain), it can be expressed as follows:

$$Error\% = \frac{D_{overlap_0}}{D_{spp}} \cdot \frac{1}{2^{\#_{mmjt}}} \cdot 100. \tag{10}$$

where $D_{overlap_0}$ is the initial overlap of the particle after the resolution of the diffusive equation (Eq. (5)). So, the $\#_{mmjt}$ chosen to obtain a given error depends on the initial overlap $D_{overlap_0}$.

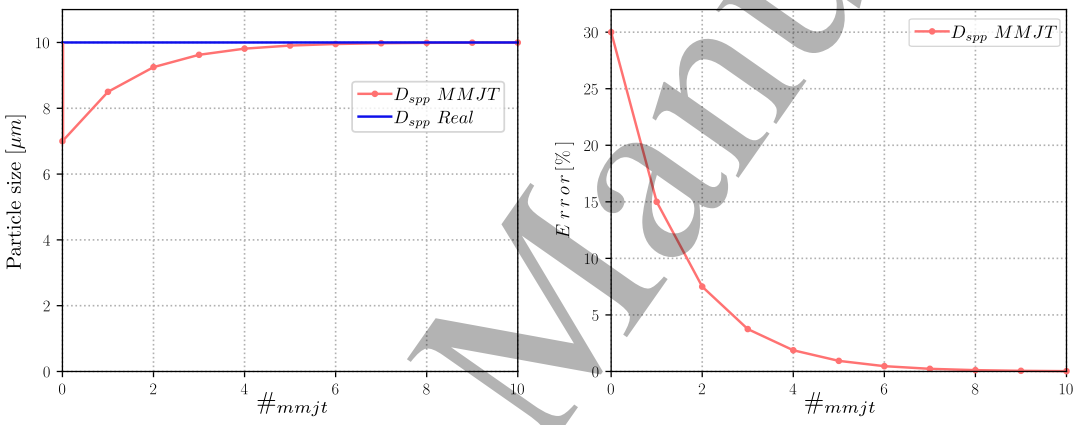

Figure 4: Internal grain diameter D_i as a function of the number of calls of Eq.(9) for a SPP with a diameter $D_{spp} = 10\mu m$.

3. Numerical results

In this section, a comparative study will be presented for different test cases. GG mechanism, in presence of spherical and irregular particles in 2D and 3D, is considered. These cases will be developed with our new formalism and compared with the former one proposed in [28, 29, 41]. Some parameters of the new methodology will be discussed, as well as, the impact of the FE mesh used.

3.1. Spherical particle

The first case corresponds to a dimensionless simulation (with an unitary reduced mobility $M\gamma = 1$). The grain (initial surface $S_0 = 0.5014$) and the particle (static radius $r_{spp} = 0.1$) are both immersed on a 2D domain of 1×1 as represented in Figure 5.

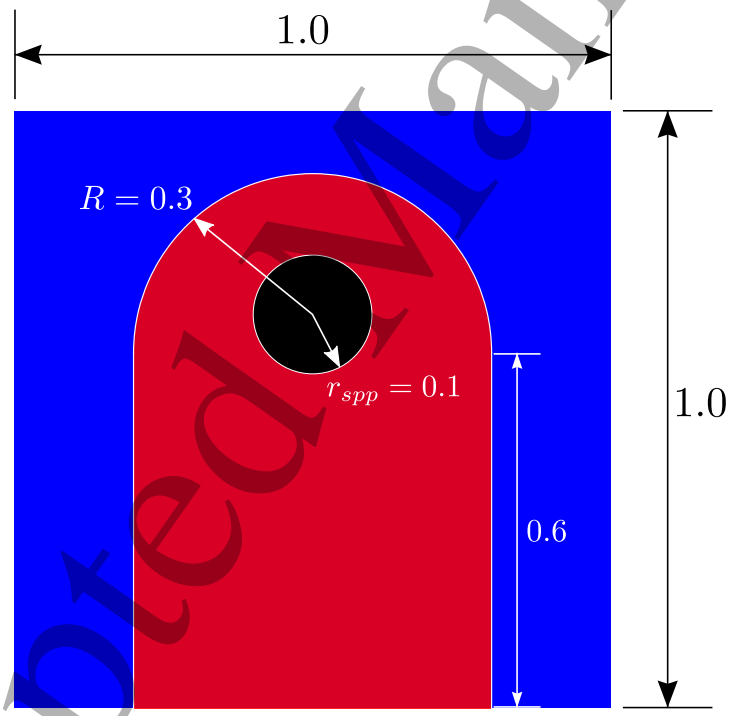

Figure 5: Initial state of a grain growth case in presence of a spherical particle.

Shrinking of the red grain and the correct interaction between the grain interface and the SPP, as a function of $\#_{mmjt}$, are investigated as illustrated in Figure 6. The use of the MMJT enables to respect progressively the correct Young-Herring equilibrium at the multiple junction between the SPP, the red grain and the blue one. This equilibrium is responsible for the abrupt modification of the local mean GB curvature (curvature in 2D and sum of the main curvatures in 3D), explaining the pinning aspect of the SPP in the mean curvature flow of the GB. Thus, the proposed methodology enables, as the former one [28], to take into account naturally the Smith-Zener effect (without the introduction of any approximated Smith-Zener driving pressure in the kinetics

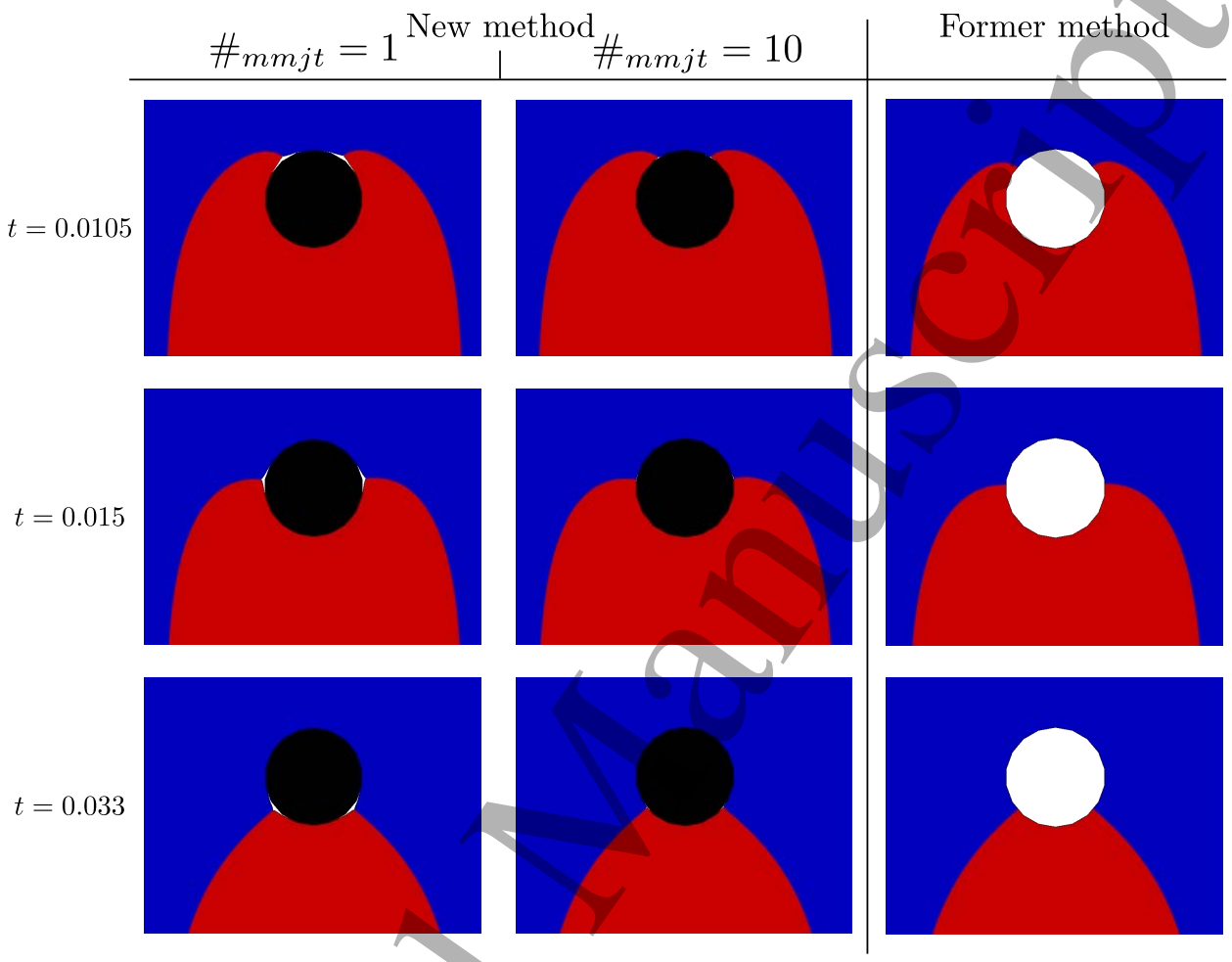

Figure 6: Comparison of the grain surface evolution for both methods at different times, to see how the red grain overpasses the particle and the influence of $\#_{mmjt}$ for the case of a grain evolution in presence of a spherical SPP with a mesh size ($h = 0.0025$).

equation Eq.(5)). As one interface is static (the SPP), the MMJT enforces progressively the orthogonality between the grain interface and the SPP (as it enforces naturally a 120/120/120 equilibrium for classical triple junctions between three evolving grains [50]). Physically, these remarks highlights that the proposed MMJT strategy is, at yet, adapted to describe only incoherent particles.

3.1.1. Mesh convergence: The mesh convergence study has been realized in both strategies, i.e. when the particles are simulated as a new distance function (Figure 7.a - New formalism) and when they are treated as holes in the domain (Figure 7.b - Former formalism [28, 29]) with an equivalent numerical strategy (same solver for the diffusive equation and time step value). Isotropic unstructured (triangular elements) FE meshes with a homogeneous mesh size h are considered, the coarsest mesh corresponds to $h = 0.025$ and the others to a refinement by a factor 2, 5 and 10 of this value. The finest with $h = 0.0025$ is considered, for each approach, as the reference case in terms

of precision. The evolution of the red grain surface of this reference case is used as an indicator of the precision and the table Tab.1 summarizes the errors obtained for both methods with the different meshes comparatively to the reference case.

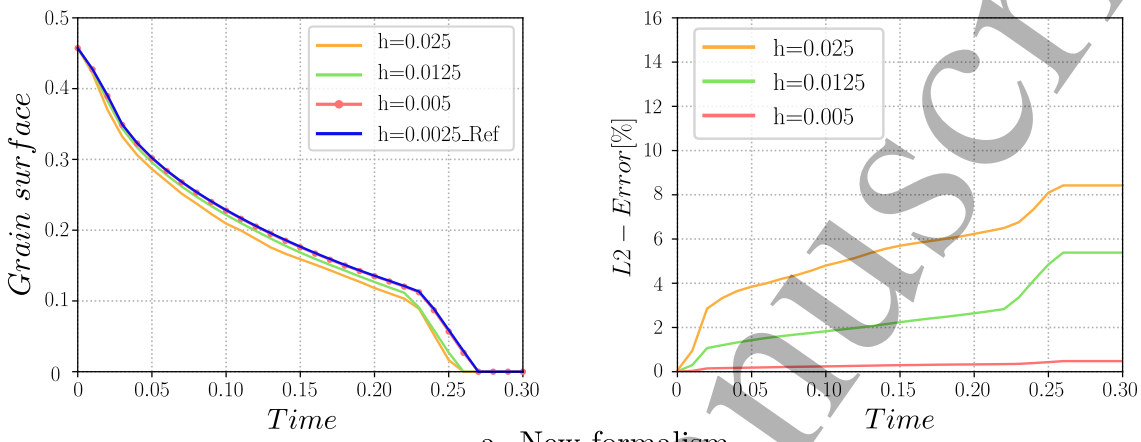

a. New formalism

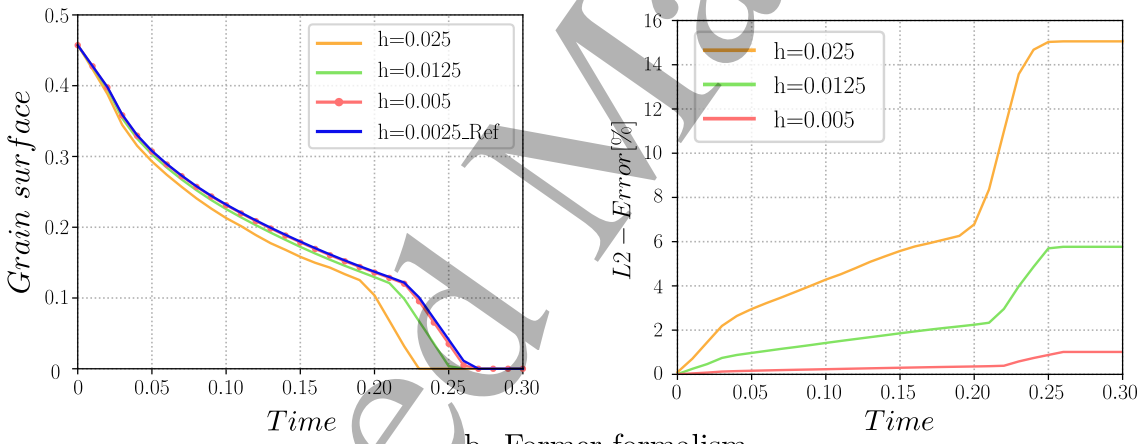

b. Former formalism

Figure 7: Mesh convergence study for the new and former formalism concerning the red grain. Surface evolution in presence of a spherical and static SPP. (see Figure 5).

As a result of this analysis, we observe a greater influence of the mesh size in the former formalism that presented an error of 15.06% against 8.42% in the new formalism for the coarsest mesh. These results validate the accuracy of the new method in terms of spatial resolution.

Mesh size	New formalism	Former formalism
h=0.025	8.42	15.06
h=0.0125	5.38	5.77
h=0.005	0.48	1.01

Table 1: Surface error [%] comparatively to the reference case ($h = 0.0025$).

3.1.2. Impact of $\#_{mmjt}$: As established in section 2.3, to well describe the grain/particle interface it is necessary to apply several times (in the same increment) the MMJT to properly respect the orthogonal condition at the grain/particle boundary.

For a given mesh size we applied the MMJT method 1, 2, 3, 4 and 10 times to establish how many iterations are needed to well represent the grain/particle interaction. Figure 8 illustrates the results obtained and the residual error by comparison with the case where $\#_{mmjt} = 10$ (reference value for each mesh size).

We can deduce from Figure 8, that this parameter could induce some errors when the mesh size is coarse. Nevertheless, for reasonable mesh size, the convergence in terms of $\#_{mmjt}$ is very fast.

3.1.3. Comparison of the new and former formalism: For the new formalism, the reference value in each case (different mesh size) is defined as the simulation obtained for a $\#_{mmjt} = 10$. These simulations were compared to the results obtained with the former method for the different mesh sizes. From Figure 9, we obtain, by considering the former method as the reference method, a maximal difference around 12% for the coarsest mesh. This difference decreases with the mesh size, reaching 3% for the finest mesh.

It must also be highlighted that the shape of the *L2* difference curves (right side of the Figures 8 and 9) can be explained by slightly different times of unpinning between both methodologies leading sometimes to a fast increase of the cumulative *L2* difference in time, but with very similar topology evolutions and obtained steady or quasi-steady states. This remark can also be applied to Figures 11, 12, 15 and 18.

This result demonstrates that the proposed methodology enables to predict correctly the SPP/GB interaction compared to the classical FE-LS treatment of Smith-Zener pinning [28, 29]. Figure 6 illustrates the evolution of the grain boundary at different stages of the simulation for the two models, the new one (right side) for which we can appreciate the influence of $\#_{mmjt}$ and the former method (left). The kinetics of the grain is well described as well as the grain/particle interaction. However, the main difference between the two methods remains a slight difference between the moment when the grain overpasses completely the particle. This difference decreases with the mesh size.

3.2. The peanut-shaped particle case

This test makes it possible, by considering an irregular peanut-shaped particle as illustrated in Figure 10, to observe if the new method enables to well describe GG mechanism when the grain boundary evolves from a concave to a convex surface. Numerical parameters are identical to the previous test case. As the mesh convergence of our model was already tested, giving a good agreement with the former method, it will not be discussed again for this configuration. Nevertheless, the study of $\#_{mmjt}$ for this concave/convex geometry remains interesting and is considered.

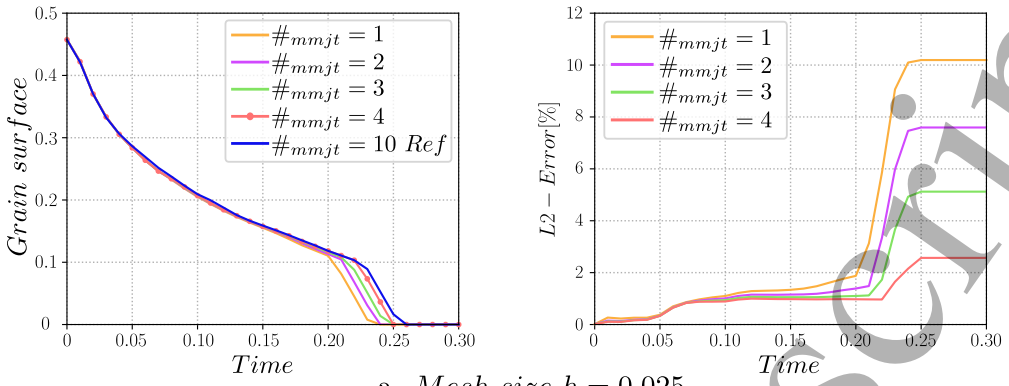

a. *Mesh size* $h = 0.025$

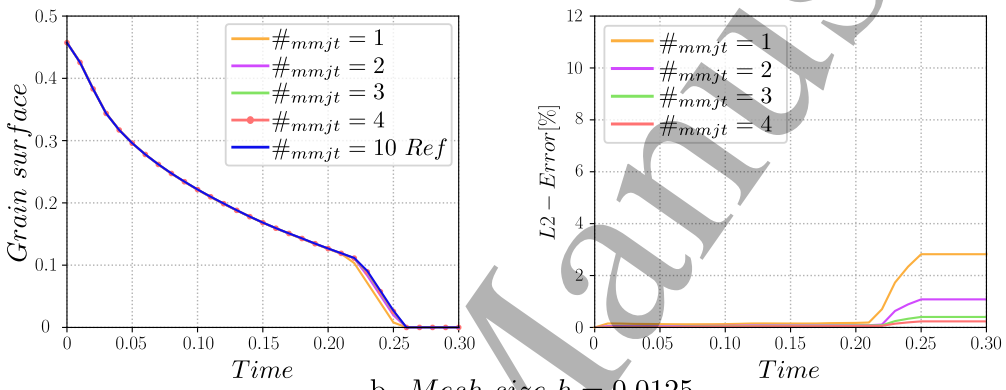

b. *Mesh size* $h = 0.0125$

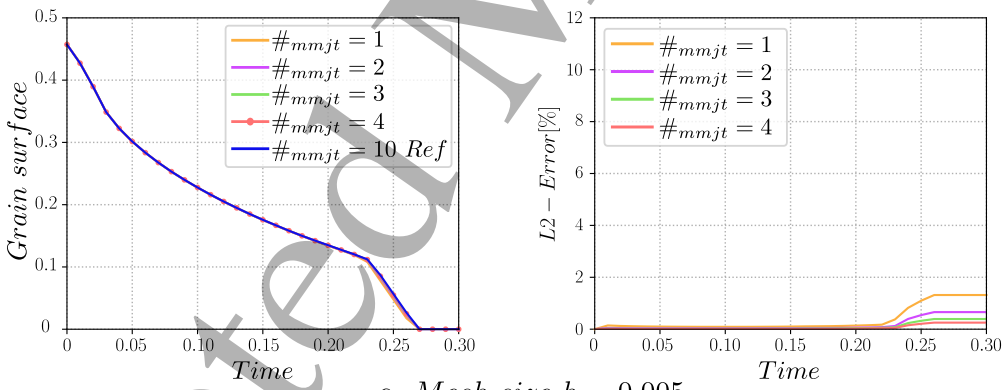

c. *Mesh size* $h = 0.005$

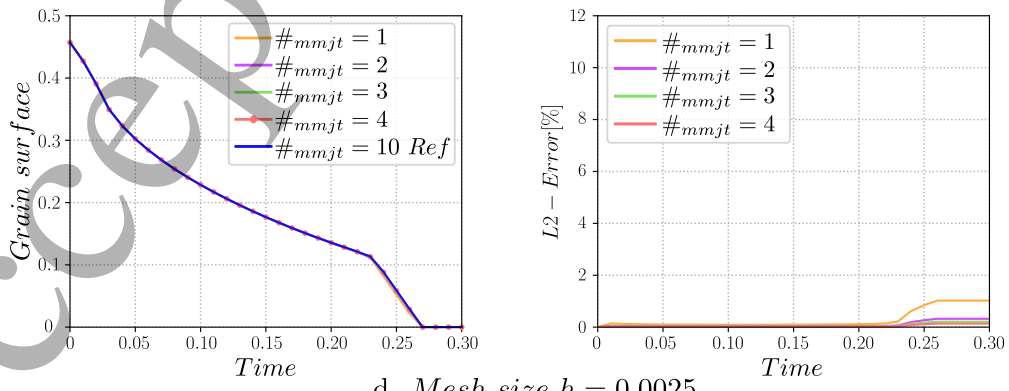

d. *Mesh size* $h = 0.0025$

Figure 8: Impact of $\#_{mmjt}$ for different mesh sizes: a. h=0.025, b. h=0.0125, c. h=0.005, d. h=0.0025 and their respective error *L2* compared with the reference value ($\#_{mmjt} = 10$).

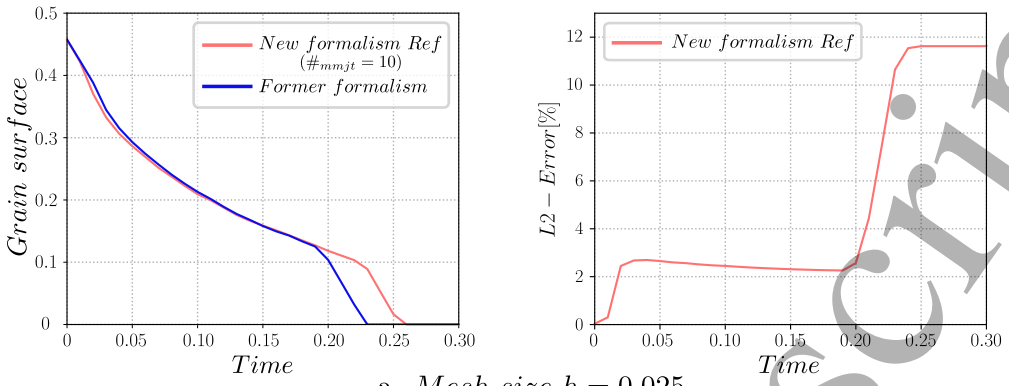

a. *Mesh size* $h = 0.025$

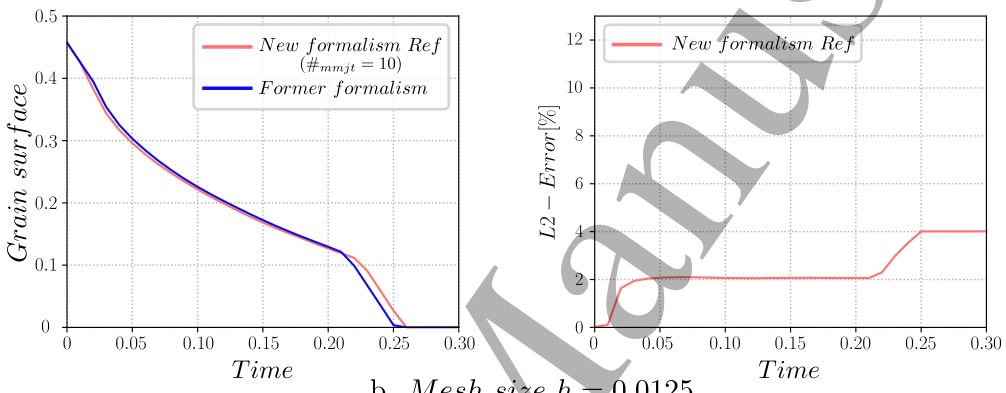

b. *Mesh size* $h = 0.0125$

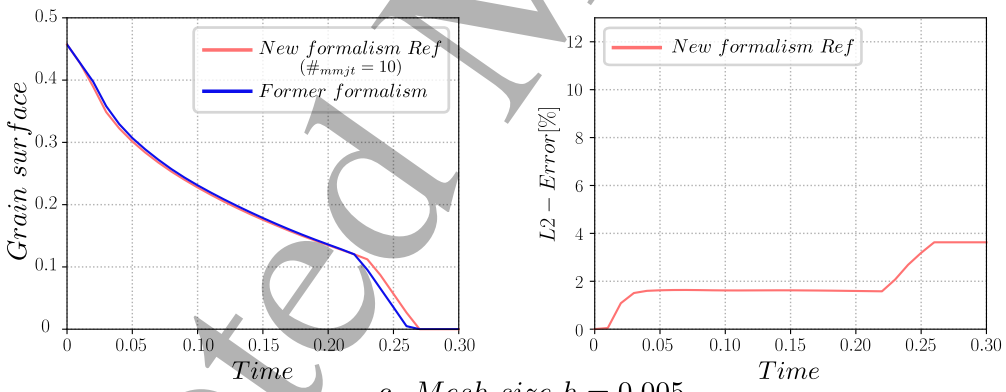

c. *Mesh size* $h = 0.005$

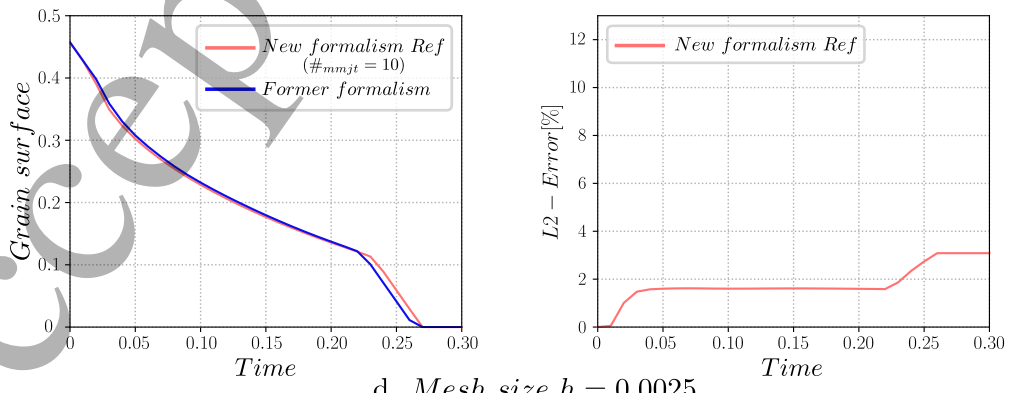

d. *Mesh size* $h = 0.0025$

Figure 9: Comparison of the grain surface evolution for the two formalisms with different mesh sizes and the corresponding *L2* difference by considering the former method as the reference.

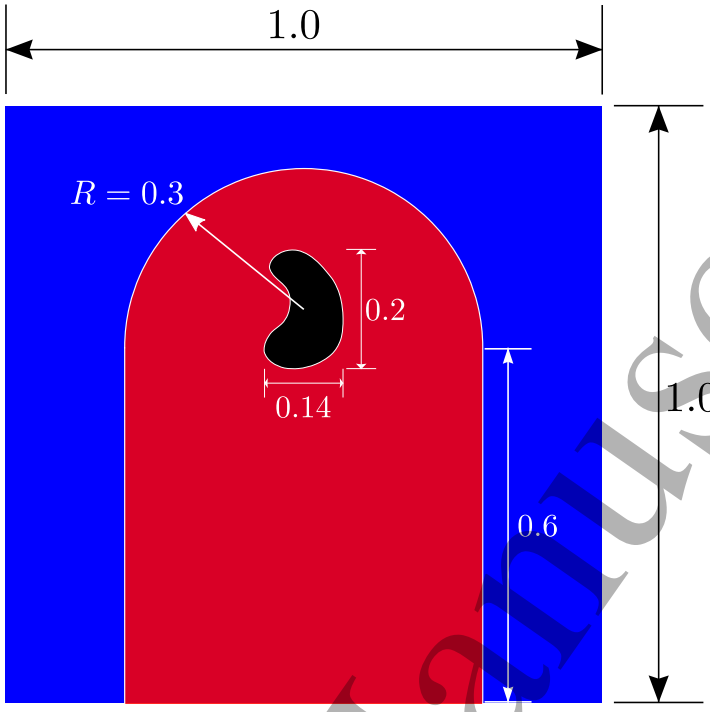

Figure 10: Initial state of the peanut-shaped particle case.

3.2.1. Precision of the new formalism: According to the findings for the spherical particle, the number of calls of Eq.(9) does not have a great impact on the description of the grain surface evolution and the produced error is reduced with the mesh size.

In Figure 11, one can see the grain surface evolution for different values of $\#_{mmjt}$ and the error produced compared with the reference value ($\#_{mmjt} = 10$) for a coarse mesh $h = 0.025$ (Figure 11.a) and for a fine mesh $h = 0.0025$ (Figure 11.b). In the first case, we obtain an error below 5% and the error is reduced to 3% for the second one. These results validate the hypothesis that the $\#_{mmjt}$ does not affect significantly the GG kinetics.

3.2.2. Comparison of the new and former formalism: The comparison of the two models is made for a coarse and a fine mesh (see Figure 12). We obtain a maximal error of 7.86% for the coarse mesh and of 2.82% for the fine one by considering the former approach as the reference case. The grain boundary evolution of both methods is represented in Figure 13, for the finest mesh ($h = 0.0025$) case. We can observe the impact of $\#_{mmjt}$ for the new method (left side) and the former one (right side). A very similar evolution of the grain interface around the peanut-shaped particle is obtained for the reference value of the new formalism compared with the former one.

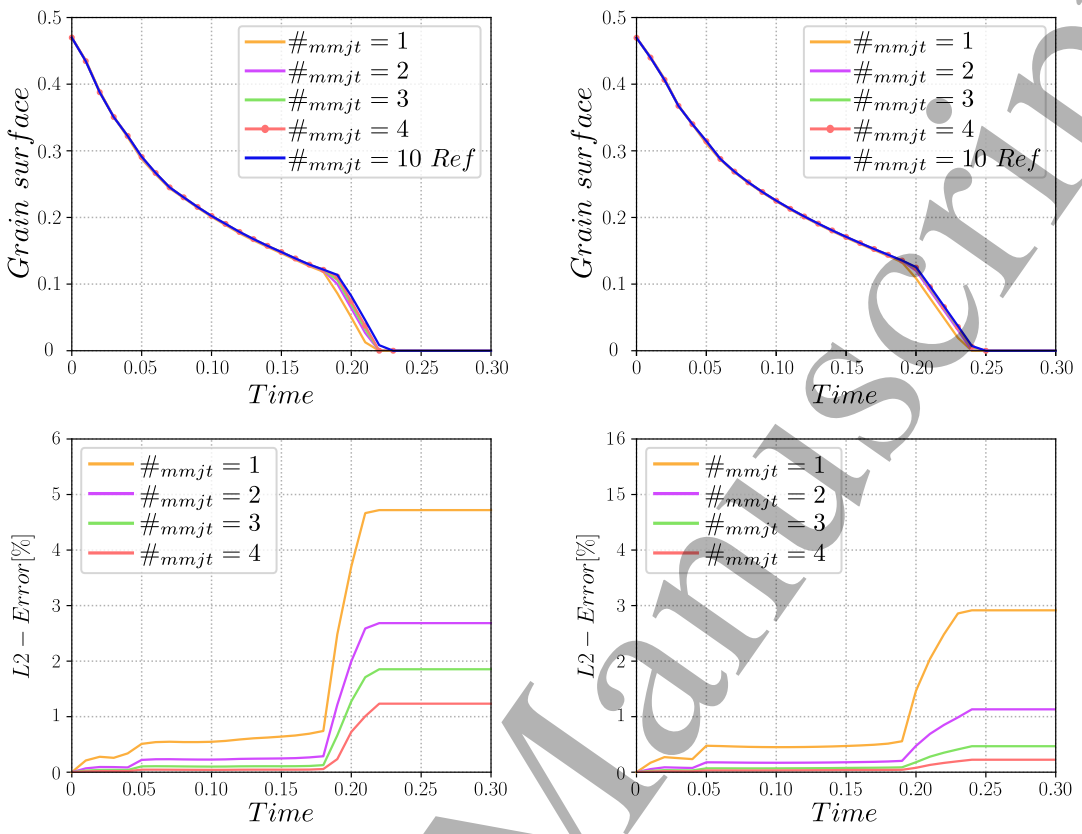

a. *Mesh size* $h = 0.025$ b. *Mesh size* $h = 0.0025$

Figure 11: Impact of $\#_{mmjt}$ for different mesh size a. h=0.025, b. h=0.0025, and their respective *L2* error for the peanut-shaped particle case.

3.3. 2D/3D cloud of particles cases

A first 2D case is considered to test the kinetic behavior of our new method in presence of several circular particles and to compare it again with the former method. The simulation domain corresponds to a dimensionless square of 1×1. We consider one grain interface (red dome) in presence of several spherical particles of different sizes as illustrated in Figure 14. An unitary reduced mobility is considered, the initial grain surface is $S_0 = 0.7413$ whereas the radius of particles varies from $r_{spp} = 0.02$ to $r_{spp} = 0.03$ and an isotropic mesh size $h = 0.005$ is considered.

In Figure 14, one can observe the grain interface at different times for both approaches. The results are very similar. The comparison of the grain surface evolution is detailed in Figure 15. The difference between the models is more significant when the grain encounters most of the particles. The grain surface presents a maximal difference around 10% which begins to decrease when the grain approaches the equilibrium state (total pinning of the grain interface as illustrated in the last picture Figure 14.e). Once again, these results illustrate that, if the new and former methods can present a slight difference in terms of kinetics of grains interacting with SPPs, this difference remains

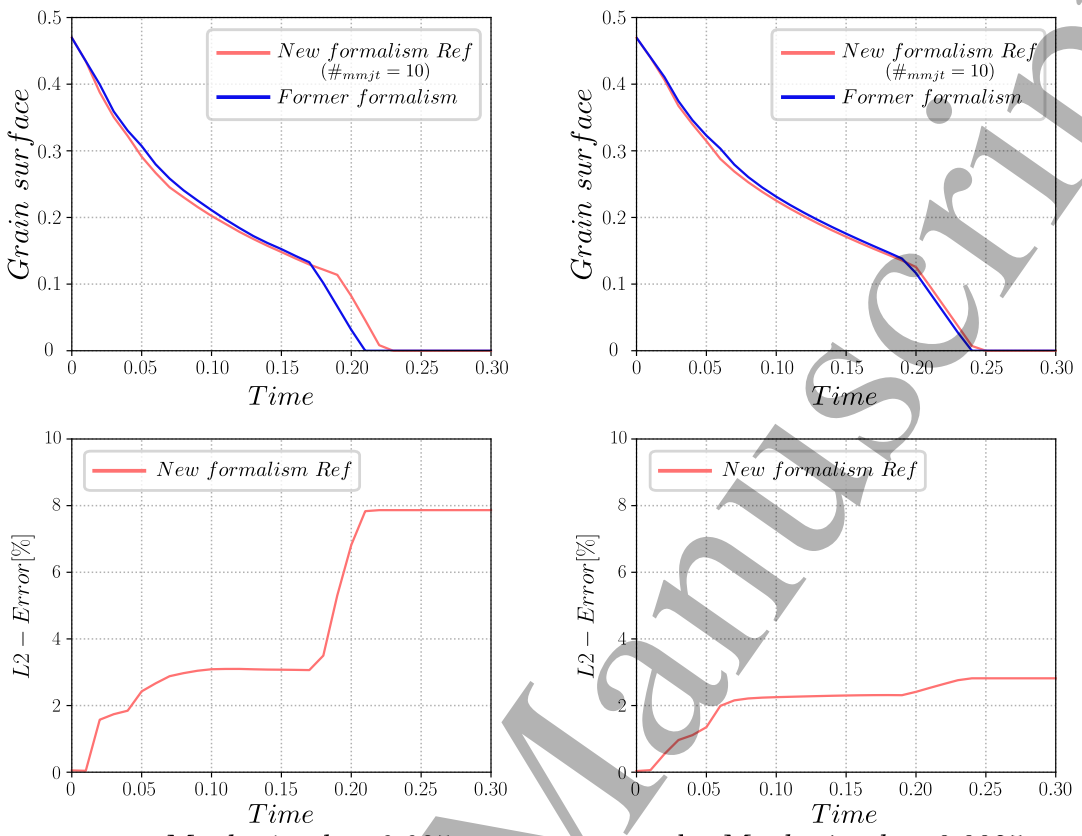

a. *Mesh size* $h = 0.025$ b. *Mesh size* $h = 0.0025$

Figure 12: Comparison of the grain surface evolution for the two formalisms for two different mesh sizes: a. the coarse mesh $h = 0.025$, b. the finest mesh $h = 0.0025$ and the corresponding *L2* errors for each peanut-shaped particle case taking the former formalism as the reference.

scarce and does not influence the equilibrium angles between GB and SPP or the quasi-static equilibrium resulting from this interaction.

The last case of this section was realized to confirm that the proposed new methodology is also totally usable in a 3D context. Thus, a similar 3D configuration (see Figure 16) of the previous test case is considered. In Figure 17, one can observe the comparative evolution for different times and view angles. Once again, from these images, we can appreciate the strong similarity between both simulations. The grain volume evolution is presented in Figure 18, as well as the *L2* difference (below 2%).

One can conclude this part by the fact that the proposed new methodology is able, for static SPPs, to perform similar simulations than the one proposed in [28, 29, 41] in 2D and 3D cases. Thus, more complex configurations, with an evolution of the SPPs can be now considered.

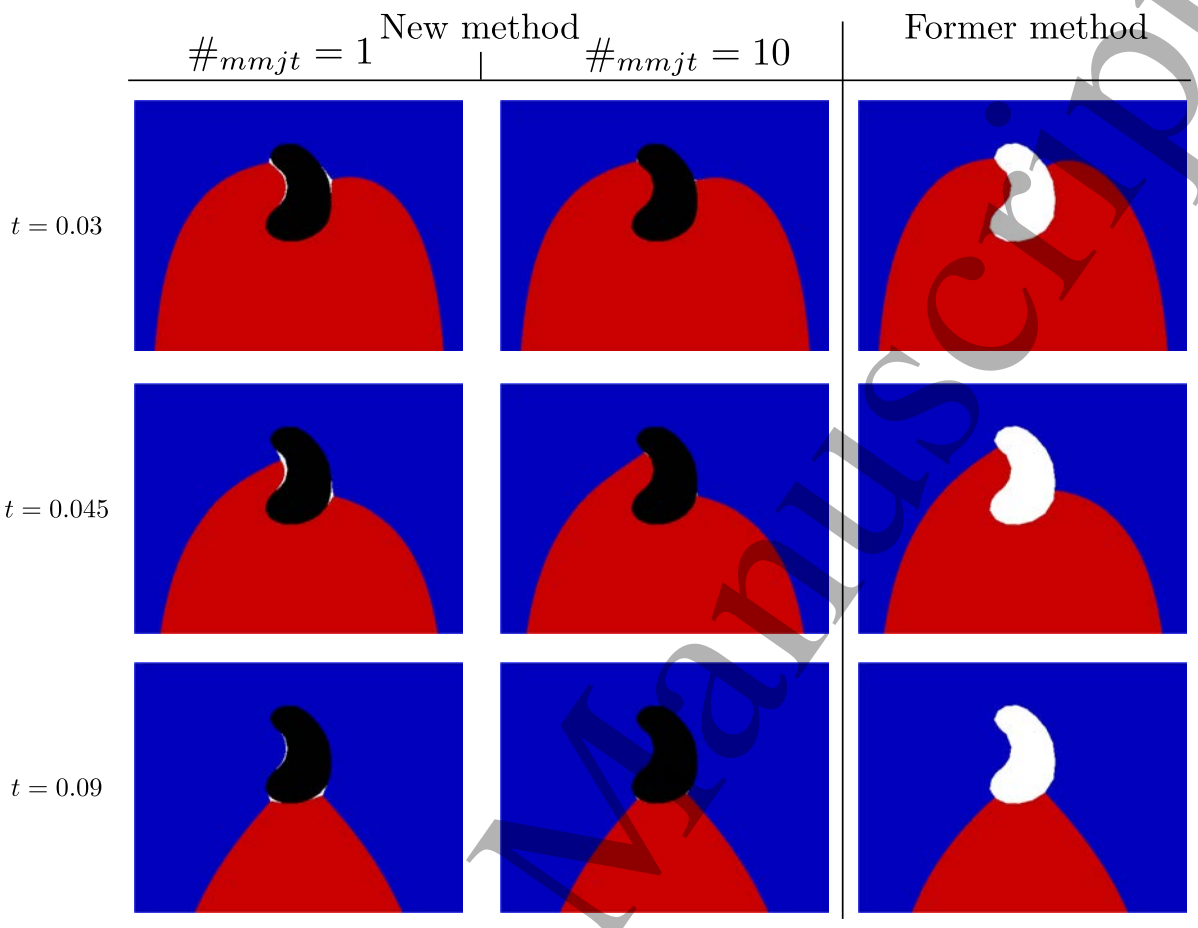

Figure 13: Comparison of the grain surface evolution for the two formalisms at different times, to appreciate the influence of $\#_{mmjt}$ for the proposed method for the peanut-shaped particle case for the finest mesh size ($h = 0.0025$).

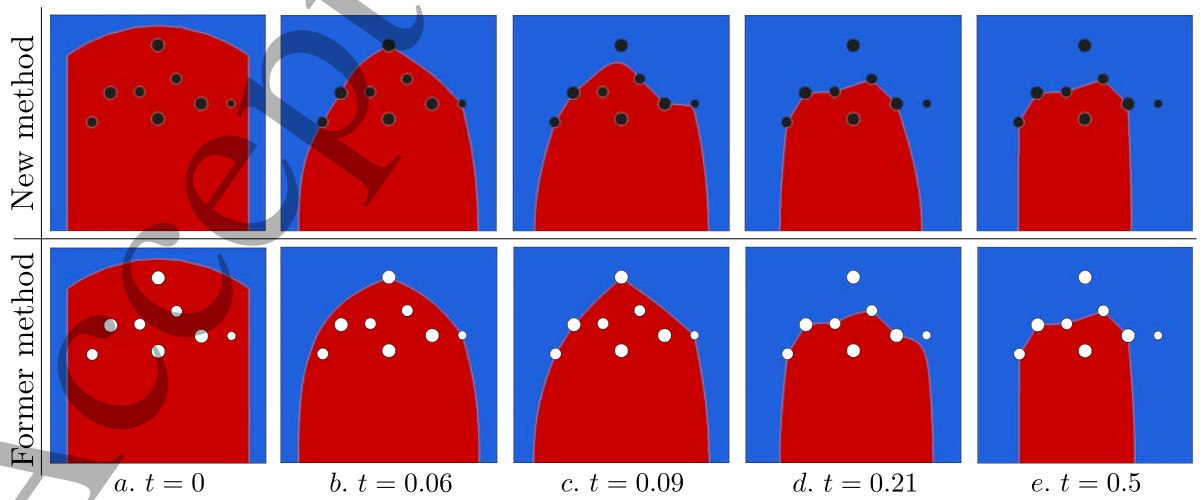

Figure 14: Comparison of the grain surface evolution in presence of multiples spherical particles for the two formalism at different times.

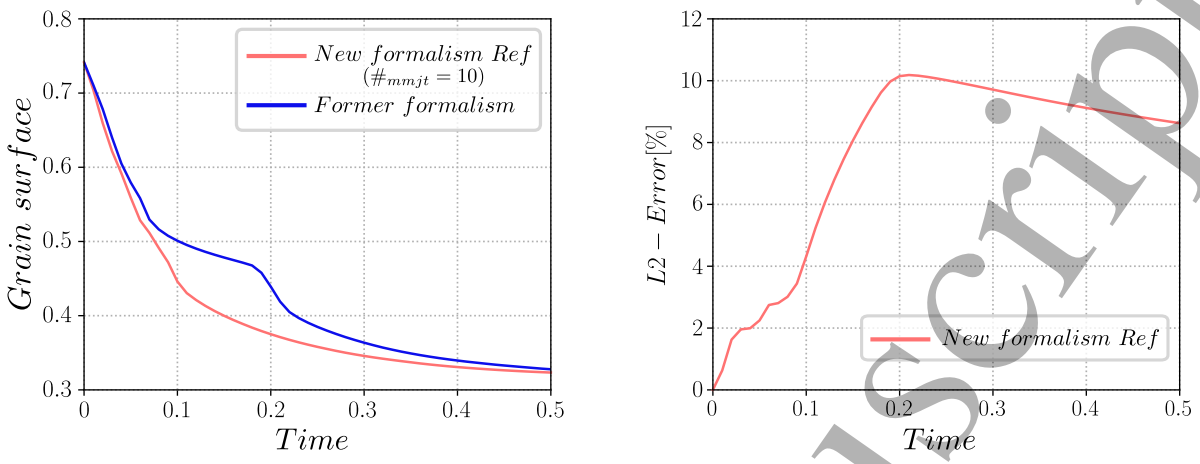

Figure 15: Comparison of the grain surface evolution for the two formalisms and the *L2* difference obtained for the grain surface between the new formalism and the former one for the 2D multiparticles case.

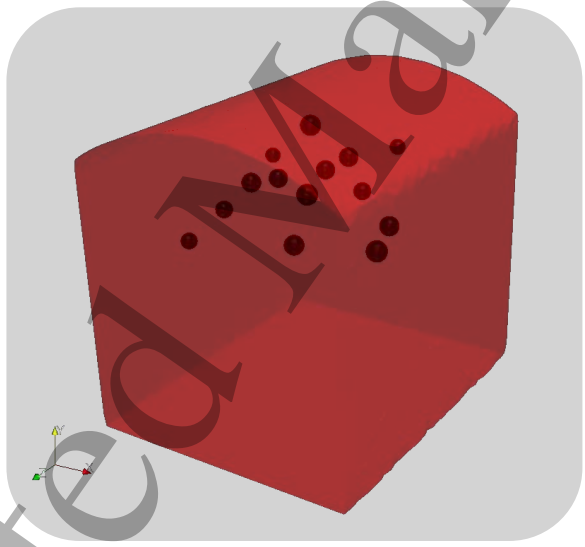

Figure 16: Initial state of the 3D case, a grain in presence of a cloud of particles.

4. Particle dissolution

As a real thermomechanical route generally involves a large variation of temperature, modelling the SPPs evolution can be important if one wants to predict quantitatively and qualitatively the microstructure evolution, notably the grain size distribution. Therefore, being able to model evolving particles during GG is necessary to treat real industrial processes and to predict accurately microstructural evolution.

To our knowledge, in the context of the LS method, the SPPs have only been simulated as static objects [28, 29, 41] and represented as holes. In the following, one strategy to take into account the evolution of the particles based on the new method previously described is proposed. Finally, this strategy will be tested by considering a

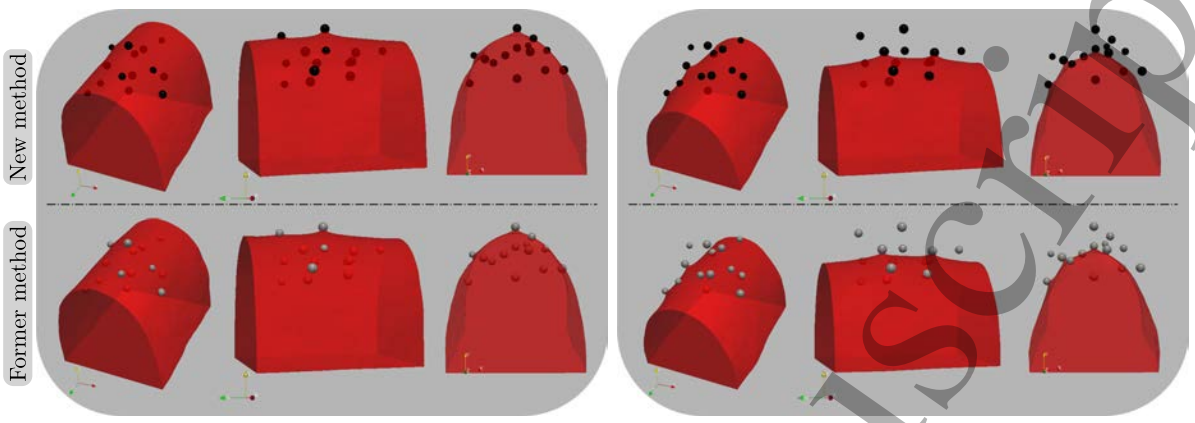

a. $t = 0.037$ *b.* $t = 0.069$

Figure 17: Comparison of the grain volume evolution for the two formalisms at different times and views (lateral and frontal) for the 3D multiparticles case.

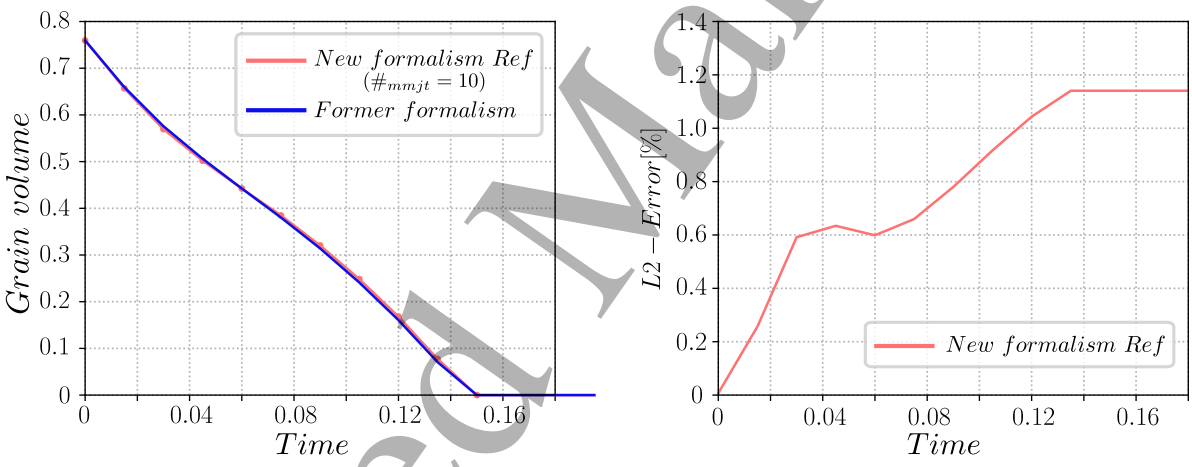

Figure 18: Comparison of the grain volume evolution for the new and former formalism with the *L2* difference obtained for the grain volume in each formalism.

realistic 2D GG case with evolving SPPs.

4.1. Evolving SPPs

Once the initial mesh is generated, the polycrystal can be created statistically or experimentally from an EBDS map. Then the grains fields φ_i are modified to introduce the new particles field φ_{SPP} (see Figure 2). A convective equation Eq.(3) is applied to φ_{SPP}: a velocity v_{spp} is computed thanks to prescribed data concerning the radius temporal evolution of the particles, then, a smoothed velocity field v is computed via a Laplacian equation (Eq.(12)) with Dirichlet boundary conditions v_{spp} established at the particle interfaces. Finally v is used to compute the velocity field $\vec{v}$ oriented towards

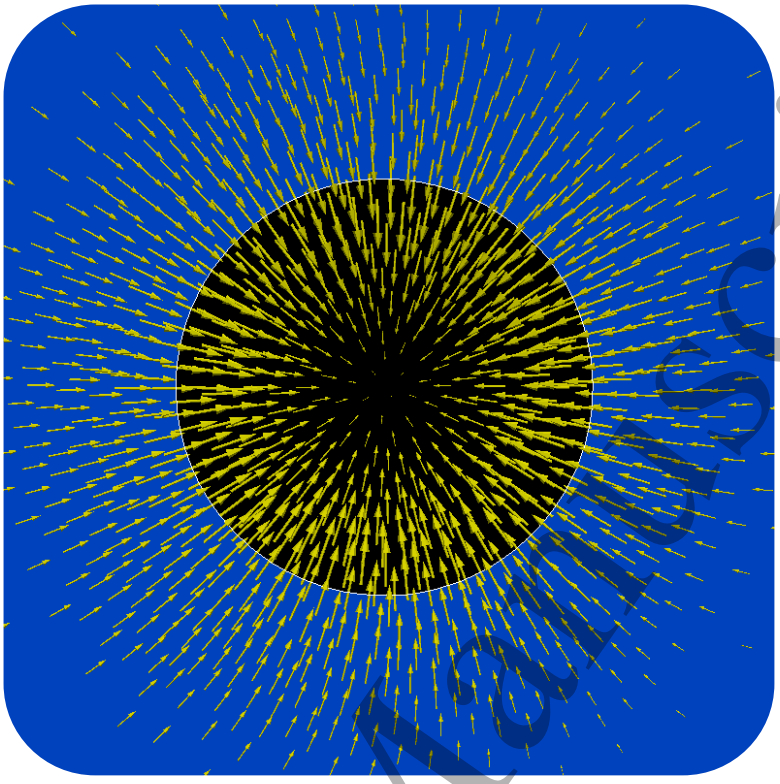

Figure 19: Example of a smoothed particle velocity ($\vec{v}$) for a spherical particle (black circle)

the center of each precipitate to be applied to φ_{SPP} (see Figure 19 for an example):

$$\begin{cases} \Delta v = 0 \\ v = v_{spp} \quad at \quad \Gamma_{spp} \end{cases} \tag{11}$$

and

$$\vec{v} = v \cdot \vec{n} = -v \cdot \nabla \varphi_{SPP}, \tag{12}$$

with $\vec{n}$ the unitary inside normal vector to the SPP, v_{spp} the velocity that we want to impose to the SPPs and $\vec{v}$ the resulting velocity field that we really impose, through a convection equation to φ_{SPP}.

All this process is made at each increment of the simulation. The smoothed velocity is implemented to reduce/eliminate the instabilities produced by the solution of the local convective finite element problem and to reduce the concentration of the isovalues of the level set function around the particles. A reinitialization of φ_{SPP} is also required at each time step to ensure the good description of the particles isovalues at each increment.

The solution of the diffusive Eq.(5) is now applied to the grains, followed by several calls of the MMJT given by the Eq.(9) to correct the overlaps and vacuums generated at the multiple junctions between grains and between grains and particles. Finally, the procedure ends with the recoloring technique and the GLS reinitialization.

4.2. Grain growth polycrystal case with random SPPs distribution

The initial microstructure is composed of around 50000 grains generated with a Laguerre-Voronoi tessellation [51]. The mean grain radius (in number) $\bar{R}$ is equal to 5 μm and an initial polydisperse spherical particle population with a surface fraction $f_{spp} = 6\%$ (around 19000 SPPs) is generated. All SPPs are assumed incoherent. Figure 20 illustrates the initial state of a domain of $200\mu m$ x $200\mu m$. The values of M and γ are chosen as representative of the $AD730^{TM}$ nickel base superalloy and come from the database of the DIGIMU© software [52]. The mobility M is then expressed as an Arrhenius law and depends on the temperature T, i.e. $M = M_0 * e^{-Q/RT}$ where M_0 is a constant $M_0 = 2.981 \cdot 10^{14}$ $[mm^4/Js]$, Q is the thermal apparent activation energy for mobility $Q = 3.87 \cdot 10^5$ $[J/mol]$, R is the ideal gas constant $R = 8.314$ $[J/(molK)]$, T is the absolute temperature, γ is assumed as constant ($6 \cdot 10^{-7}$ $[J/mm^2]$) and the γ' solvus temperature $T_{\gamma'_{solvus}}$ is estimated at around 1110 $[°C]$.

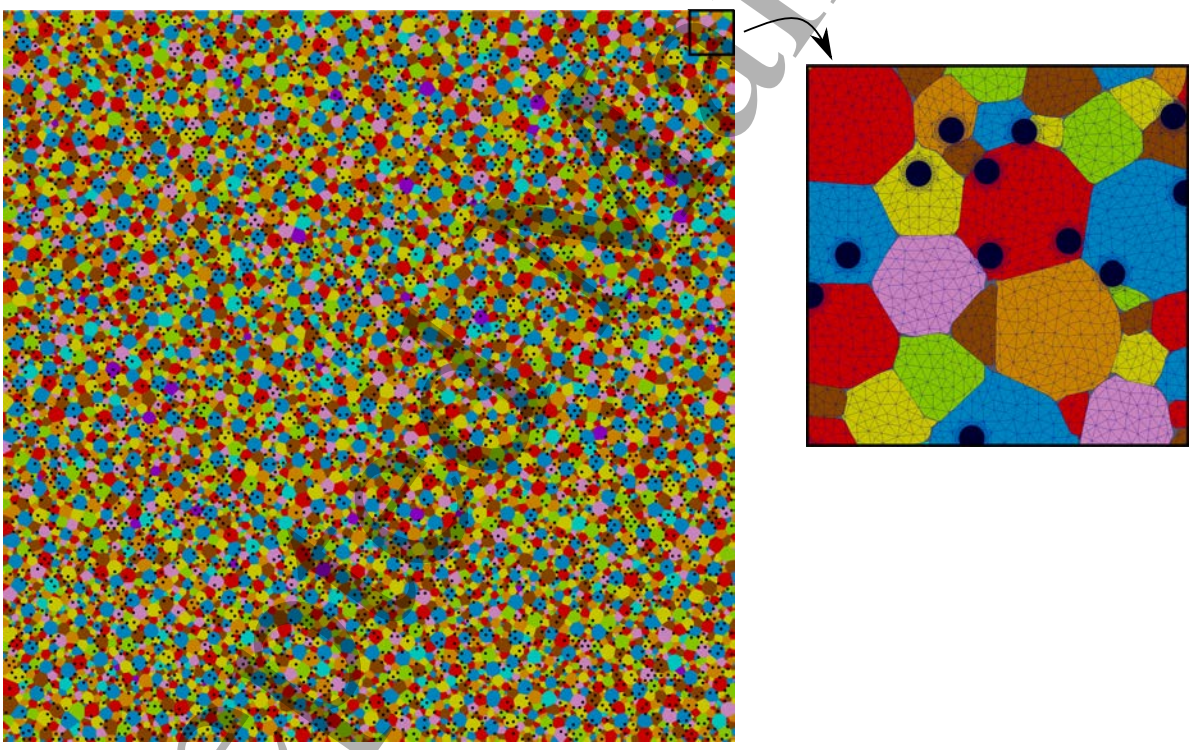

Figure 20: Initial state of the microstructure: the mesh is refined on around the SPP interfaces. SPPs are treated thanks to a LS field.

A thermal treatment of $t = 3$ $[h]$ is considered. More precisely, an isothermal treatment at 990 $[°C]$ for 45 $[min]$ is followed by a linear increase of the temperature until 1120 $[°C]$ in 90 $[min]$ and the material is maintained at this temperature for others 45 $[min]$ (Figure 23.a). The main interest of such thermal treatment is to clearly see the SPP evolution near the solvus temperature (for the reference case), and also, to simulate different particles dissolution velocities that consequently produce different effective solvus temperatures (total disappearance of SPPs in full field simulations) and

to study the impact on such evolution on the mean grain size evolution.
An empiric particle velocity v_{spp} is defined here as $v_{spp} = \beta \cdot (T - 990)$ where β $[mm \cdot s^{-1} \cdot^{\circ} C^{-1}]$ is a constant that we made vary from 10^{-9} to 0 to appreciate the complete particle dissolution at different rates (Figure 23.b). A such totally empiric expression enables here to illustrate the capabilities of our methodology for a large range of v_{spp} without the precise use of experimental data for SPPs disappearance velocity.

The time step for the simulation was set to 5 $[s]$ which is small enough to correctly describe the interactions between the GBs and the particle interfaces. The Figures 21 and 22 illustrate the evolution of the microstructure at different stages of the simulation (2700, 5400, 8100 and 10800 [s]) for our reference case ($\beta = 10^{-9}$ $[mm \cdot s^{-1} \cdot^{\circ} C^{-1}]$), showing how the particles disappear during the thermal treatment and the concomitant grain boundary network evolution (pinning followed by classical GG).

Figure 23.c shows the particle surface evolution as a function of time. For the reference case ($\beta = 10^{-9}$ $[mm \cdot s^{-1} \cdot^{\circ} C^{-1}]$), the F_{spp} is static for the first 45 $[min]$ and then completely dissolved near the effective solvus temperature (~ 1120 $[^{\circ}C]$). When the parameter β increases, the particles velocity also increases and the particles dissolve faster. Thus, the effective $T_{\gamma'_{solvus}}$ decreases when the parameter β increases (see Figure 23.d).

Finally, Figure 23.e illustrates the mean grain surface. Considering the reference case, at the beginning of the simulation, the grains are pinned by the particles and there is not significant GG, but then when the particles start to dissolve, the grains start to grow and finally, when no more particles remain the grains can grow freely as for classical GG mechanism. When the constant β increases, the particles dissolve in less time, enabling the grains to grow freely earlier than in the reference case. When $\beta = 0$ $[mm \cdot s^{-1} \cdot^{\circ} C^{-1}]$ (null SPP velocity) the particles fraction is fixed for all the simulation and it can be appreciated how the particles block the GG, resulting in a large difference of the mean grain size at the end of the simulation (see Figure 23.e).

The mean grain size evolution in function of β illustrates here how it will be possible to play with a thermal treatment near the solvus temperature while keeping a reasonable impact on the GG kinetics.

Such aspect has of course a strong industrial interest. A simple and imposed v_{spp} profile was proposed here as an illustration, but the methodology proposed in Eqs.(11) and (12) will be directly usable with more complex evolution laws or data directly coming from experimental observations.

The computation time for the 50000 initial grains took 67.3 [h] when performed on 24 processors which is a promising result given the high number of grains and the possibility to reproduce the particle evolution.

4.3. Grain growth polycrystal case with heterogeneous SPPs distribution

In this case, we assume a heterogeneous bimodal particle distribution, the initial microstructure is similar to the previous polycrystal. A simulation domain of $200\mu m$ x

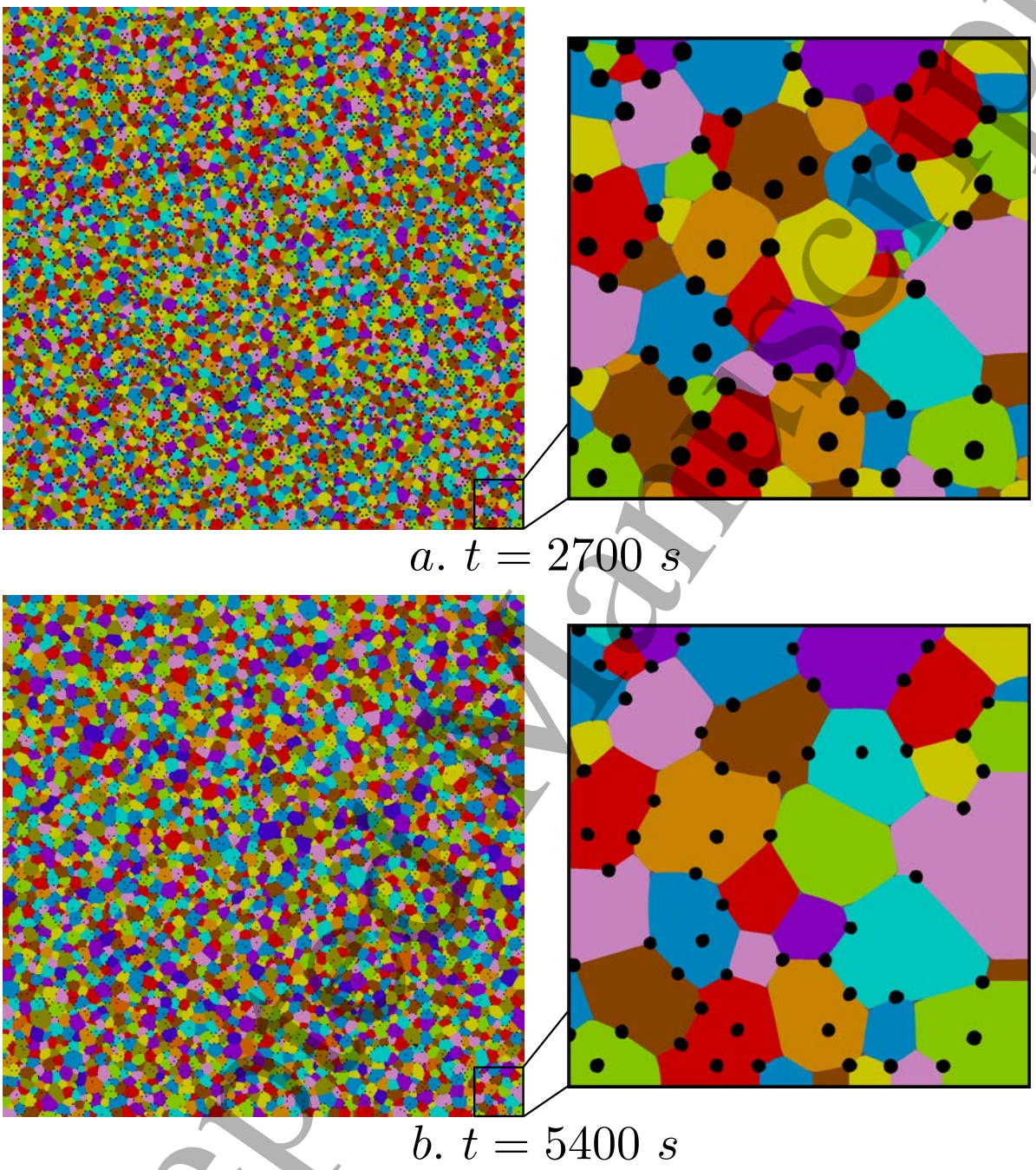

Figure 21: Microstructure evolution at different times for a random SPPs distribution.

$200\mu m$ with an initial number of grains around 50000 is considered. The mean grain radius (in number) $\bar{R} = 5\ \mu m$ and a spherical particles population with a initial surface fraction $f_{spp} = 6\%$ divided in big SPPs with $f_{spp_{big}} = 4\%$ of radius $r_{spp_{big}} = 2\ \mu m$ and small SPPs with $f_{spp_{small}} = 2\%$ of radius $r_{spp_{small}} = 1\ \mu m$, distributed in two bands in the domain as illustrated in Figure 24.a. This case is developed to illustrate the possibility of treated a heterogeneous particle population and to reproduce more accurately the real microstructure of the $AD730^{TM}$ nickel base superalloy, which is classically composed of

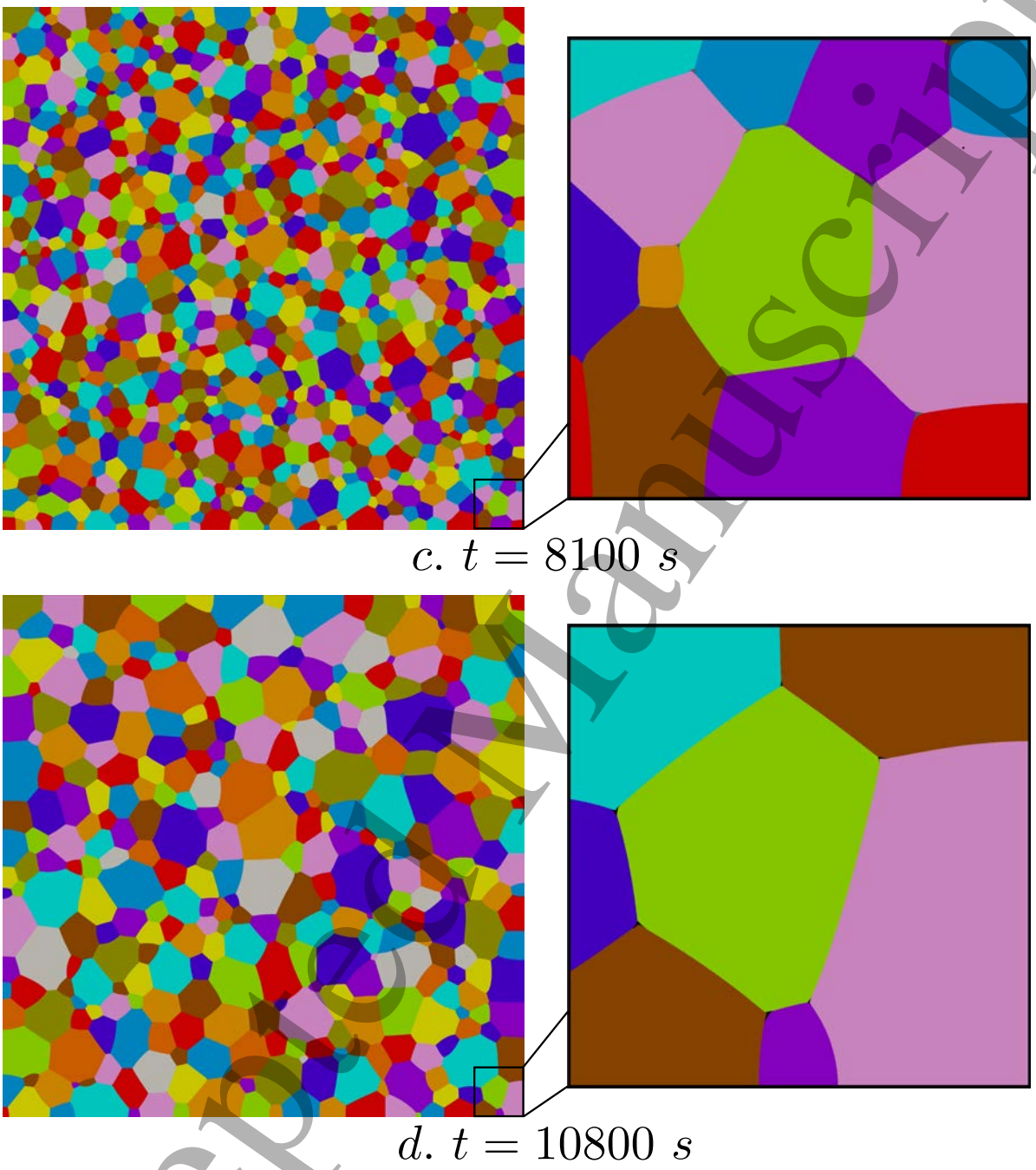

Figure 22: Microstructure evolution at different times for a random SPPs distribution.

two SPPs populations (see Figure 25) and also to observe if a heterogeneous GG can take place.

The material properties are the same as for the previous polycrystal case and the material is submitted to the same thermal treatment (see Figure 23.a).

The particle velocity v_{spp} is also established with the same kinetic law (see Figure 23.b). The small particles will be dissolved before the large particles, thus the bands regions will present a classical GG mechanism sooner than the entire domain.

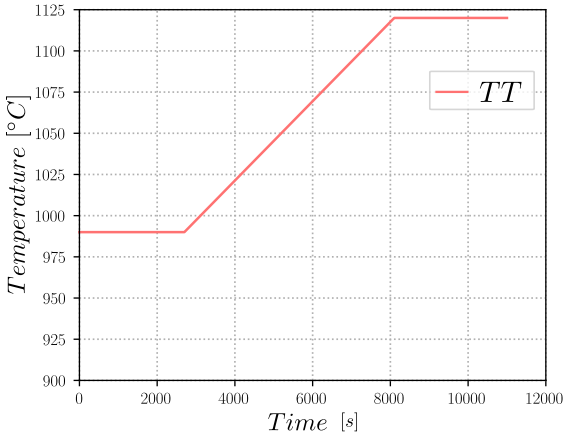

a. *Thermal treatment*

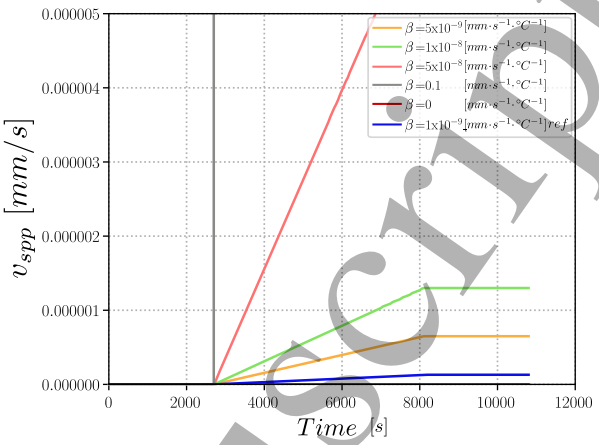

b. *Particle size evolution velocity*

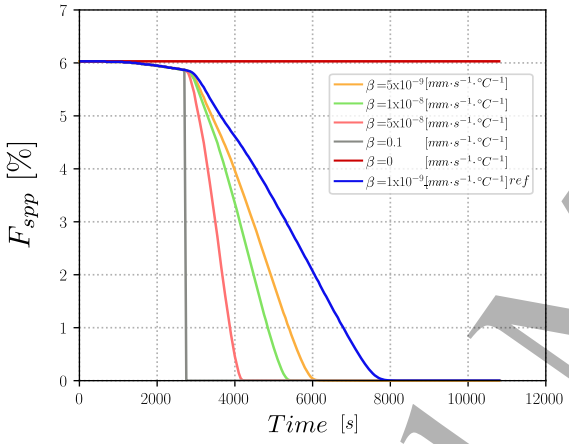

c. *Particle surface fraction*

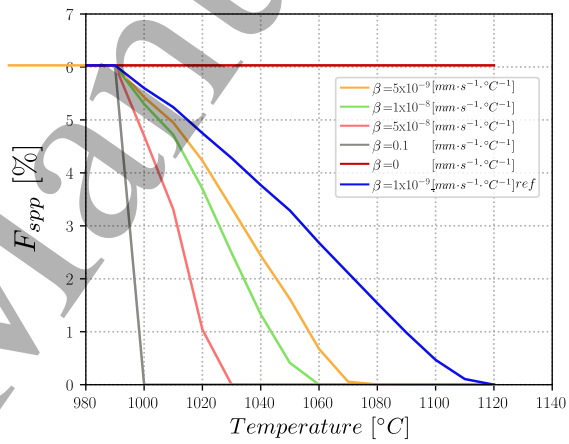

d. *Particle dissolution temperature*

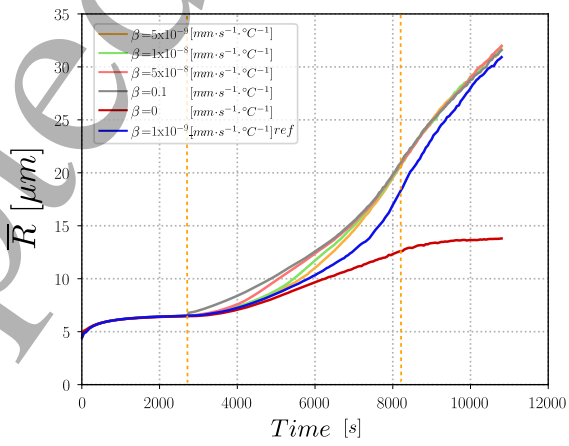

e. *Mean grain radius*

Figure 23: Results of the 2D-50000 grains case with evolving particles: comparison between the MMJT approach.

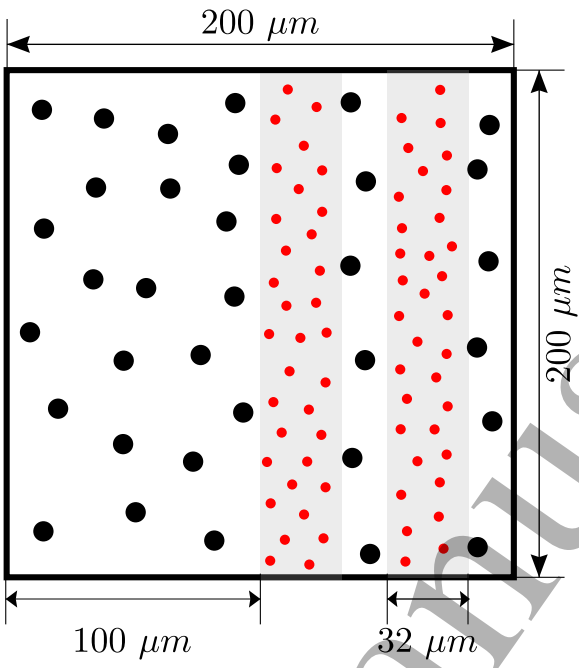

a. Initial state scheme

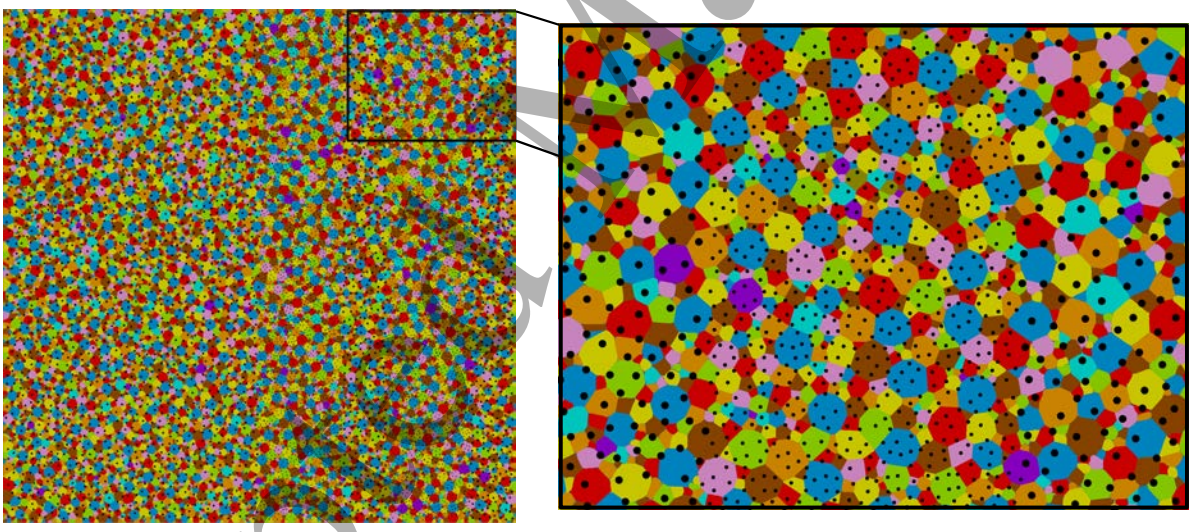

b. $t = 0\ s$

Figure 24: Schematic and simulation initial microstructure for a heterogeneous SPPs dispersion.

The Figures 26 and 27 illustrate the evolution of the microstructure at different stages of the simulation (2580, 4950, 6880 and 10800 [s]) for our reference case ($\beta = 10^{-9}$ $[mm \cdot s^{-1} \cdot {}^{\circ}C^{-1}]$), showing the particle and GG evolution during the thermal treatment.

For the initial isothermal treatment where the particles do not evolve, the grain size are smaller in the zones composed of small SPPs. This can be easily explained by a bigger resulting pinning pressure in this zone than in the zone with large SPPs (see Figure 26.a). When the temperature increases, the particles begin to dissolve and the

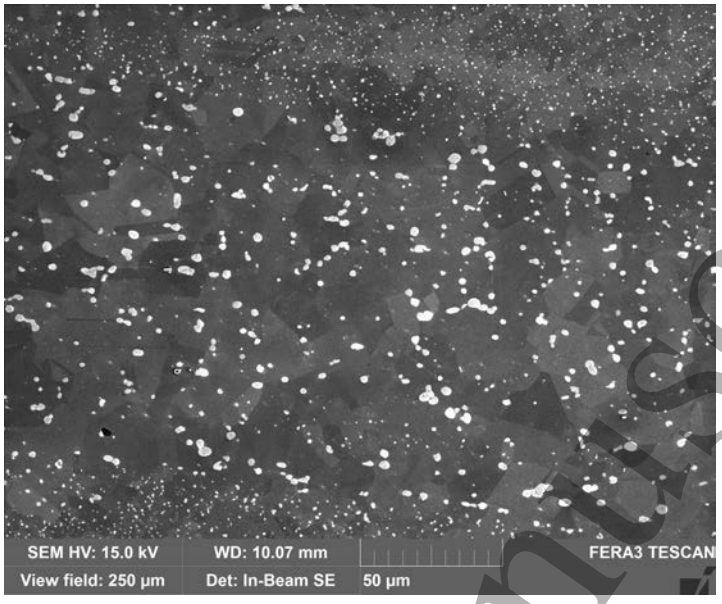

Figure 25: Classical microstructure of the $AD730^{TM}$ superalloy.

grains evolve, especially at the regions composed of small particles where the small grains of this regions begin to grow (see Figure 26.b). Once the small SPPs are completely dissolved, the grains can grow freely and as represented in Figure 26.c (white ellipses) some grains can grow more than others, thus a heterogeneous grain evolution begins to take place, where some grains are likely to grow more and more leading potentially to abnormal grain growth.

The thermal treatment ends with a maintain of temperature at 1120 $[^{\circ}C]$ which is superior to the solvus temperature, so no particles remain and all the microstructure evolves following a pure GG mechanism.

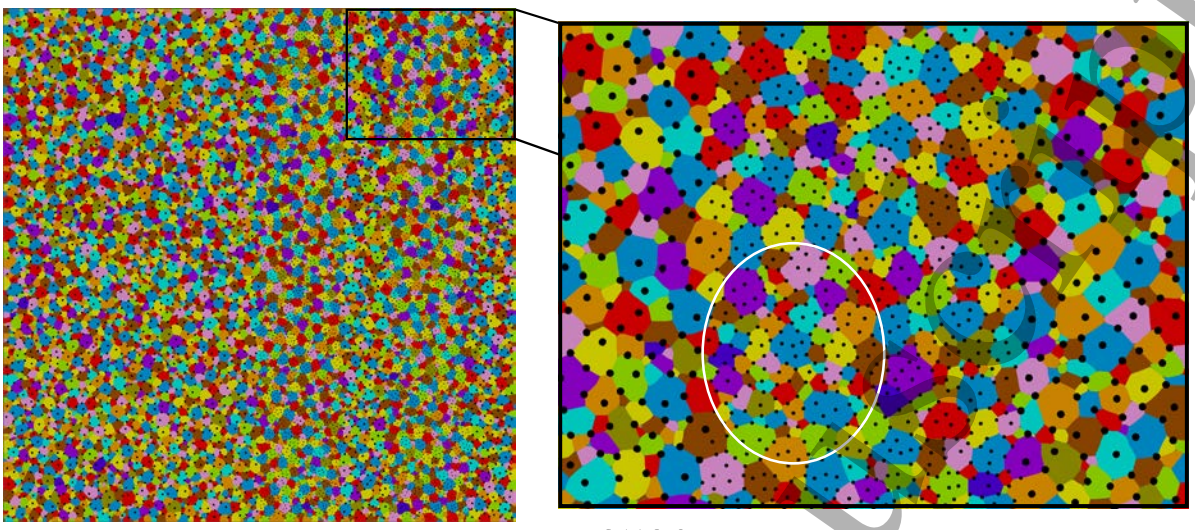

$a.\ t = 2580\ s$

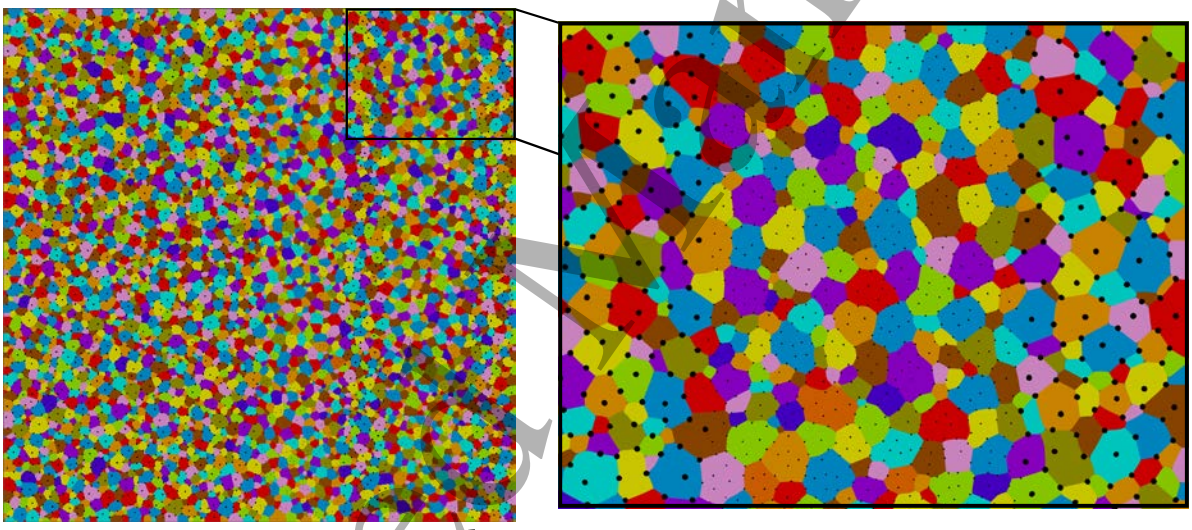

$b.\ t = 4950\ s$

Figure 26: Microstructure evolution at different times for a heterogeneous SPPs distribution.

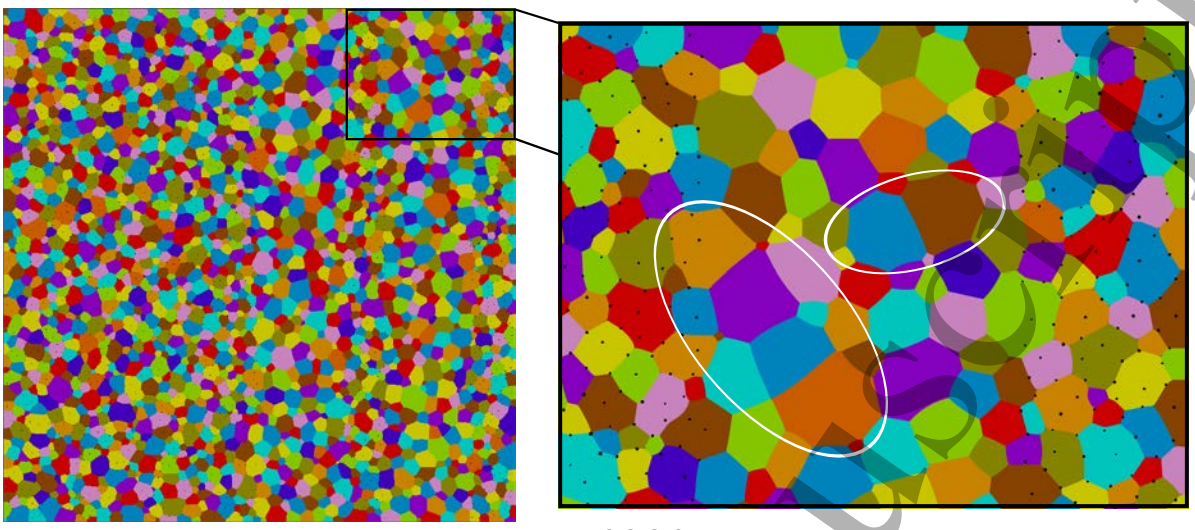

$c.\ t = 6880\ s$

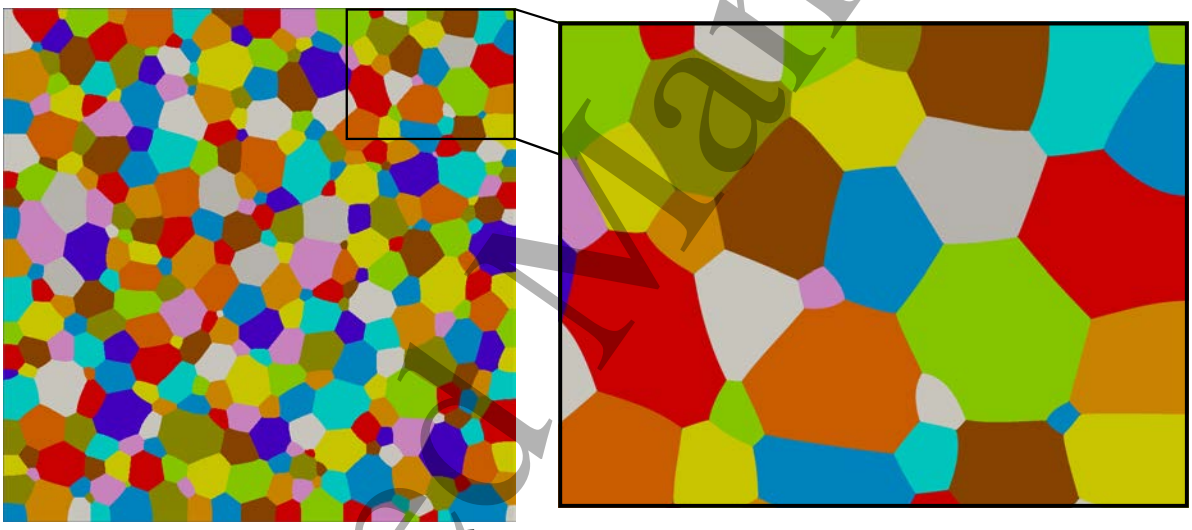

$d.\ t = 10800\ s$

Figure 27: Microstructure evolution at different times for a heterogeneous SPPs distribution.

5. Conclusions and perspectives

A new methodology to describe second phase particles in FE-LS modeling of GG was proposed. This approach was validated by comparison with a pre-existing approach.

The use of a LS function to represent SPPs enables a better integration of SPPs in the model when an evolving SPP population is considered. As opposed to SPPs described by holes in the FE mesh, this new formalism opens new perspectives regarding full field recrystallization simulations. SPPs mechanical behaviour could be modeled and it could be expected a non-negligible influence of such numerical capability on the prediction of nucleation events and recrystallization kinetics.
A first methodology has been proposed in order to take into account evolving particles in the context of a FE-LS modeling of GG.

This new capability has been illustrated for a nickel base superalloy in the context of a thermal treatment near the γ' solvus temperature. This new method provides a FE-LS framework able to accurately take into account the physical evolution of SPPs (due to dissolution/appearance of particles or Ostwald ripening) and is expected to predict quantitatively the concomitant grain size distribution and topology evolutions. Moreover, complex local heterogeneous SPPs velocities could also be investigated. Indeed, it is well known that the growth and/or dissolution of precipitates can be accelerated by the contact with evolving GBs. The proposed formalism will be adapted to numerically discuss this phenomenon.
Finally, one of our perspectives is focused on the experimental validation of the proposed numerical framework. This aspect will be on a forthcoming publication dedicated to the $AD730^{TM}$ nickel base superalloy.

Acknowledgements

The authors thank the ArcelorMittal, ASCOMETAL, AUBERT & DUVAL, CEA, FRAMATOME, SAFRAN, TIMET, Constellium and TRANSVALOR companies and the ANR for their financial support through the DIGIMU consortium and ANR industrial Chair (Grant No. ANR-16-CHIN-0001).

Data availability

The raw and processed data required to reproduce these findings cannot be shared at this time as the data also forms part of an ongoing study.

References

[1] C. Smith, Introduction to grains, phases, and interfaces - an interpretation of microstructure, Trans. AIME 175 (1948) 15–51. doi:10.1007/s11663-010-9364-6.

[2] P. Gong, E. J. Palmiere, W. M. Rainforth, Dissolution and precipitation behaviour in steels microalloyed with niobium during thermomechanical processing, Acta Materialia 97 (2015) 392–403. doi:10.1016/j.actamat.2015.06.057.

[3] S. Dépinoy, B. Marini, C. Toffolon-Masclet, F. Roch, A. F. Gourgues-Lorenzon, Austenite Grain Growth in a 2.25Cr-1Mo Vanadium-Free Steel Accounting for Zener Pinning and Solute Drag: Experimental Study and Modeling, Metallurgical and Materials Transactions A: Physical Metallurgy and Materials Science 48 (5) (2017) 2289–2300. doi:10.1007/s11661-017-4002-4.

[4] C. Zener, Theory of growth of spherical precipitates from solid solution, Journal of Applied Physics 20 (10) (1949) 950–953. doi:10.1063/1.1698258.

[5] P. A. Manohar, M. Ferry, T. Chandra, Five Decades of the Zener Equation, ISIJ International 38 (1998) (1998) 913–924. doi:10.2355/isijinternational.38.913.

[6] P. A. Manohar, D. P. Dunne, T. Chandra, C. R. Killmore, Grain growth predictions in microalloyed steels, ISIJ International 36 (2) (1996) 194–200. doi:10.2355/isijinternational.36.194.

[7] M. Miodownik, E. A. Holm, G. N. Hassold, Highly parallel computer simulations of particle pinning: zener vindicated, Scripta Materialia 42 (12) (2000) 1173–1177. doi:10.1016/S1359-6462(00)00354-7.

[8] G. Couturier, R. Doherty, C. Maurice, R. Fortunier, 3D finite element simulation of the inhibition of normal grain growth by particles, Acta Materialia 53 (4) (2005) 977–989. doi:10.1016/j.actamat.2004.10.044.

[9] N. Moelans, B. Blanpain, P. Wollants, Phase field simulations of grain growth in two-dimensional systems containing finely dispersed second-phase particles, Acta Materialia 54 (4) (2006) 1175–1184. doi:10.1016/j.actamat.2005.10.045.

[10] M. P. Anderson, G. S. Grest, R. D. Doherty, K. Li, D. J. Srolovitz, Inhibition of grain growth by second phase particles: Three dimensional Monte Carlo computer simulations, Scripta Metallurgica 23 (5) (1989) 753–758. doi:10.1016/0036-9748(89)90525-5.

[11] J. Gao, R. G. Thompson, B. R. Patterson, Computer simulation of grain growth with second phase particle pinning, Acta Materialia 45 (9) (1997) 3653–3658. doi:10.1016/S1359-6454(97)00048-7.

[12] D. J. Srolovitz, M. P. Anderson, G. S. Grest, P. S. Sahni, Computer simulation of grain growth-III. Influence of a particle dispersion, Acta Metallurgica 32 (9) (1984) 1429–1438. doi:10.1016/0001-6160(84)90089-0.

[13] C. L. Prinzio, E. Druetta, O. B. Nasello, More about Zener drag studies with Monte Carlo simulations, Modelling and Simulation in Materials Science and Engineering 21 (2). doi:10.1088/0965-0393/21/2/025007.

[14] K. R. Phaneesh, A. Bhat, P. Mukherjee, K. T. Kashyap, On the Zener limit of grain growth through 2D Monte Carlo simulation, Computational Materials Science 58 (2012) 188–191. doi:10.1016/j.commatsci.2012.02.013.

[15] D. Raabe, Introduction of a scalable three-dimensional cellular automaton with a probabilistic switching rule for the discrete mesoscale simulation of recrystallization phenomena, Philosophical Magazine A: Physics of Condensed Matter, Structure, Defects and Mechanical Properties 79 (10) (1999) 2339–2358. doi:10.1080/01418619908214288.

[16] D. Raabe, L. Hantcherli, 2D cellular automaton simulation of the recrystallization texture of an if sheet steel under consideration of Zener pinning, Computational Materials Science 34 (4) (2005) 299–313. doi:10.1016/j.commatsci.2004.12.067.

[17] A. Eivani, J. Zhou, J. Duszczyk, A new approach to incorporating the effect of nano-sized dispersoids on recrystallization inhibition into monte carlo simulation, Computational Materials Science 54 (2012) 370 – 377. doi:10.1016/j.commatsci.2011.10.016.

[18] F. Villaret, B. Hary, Y. [de Carlan], T. Baudin, R. Log, L. Maire, M. Bernacki, Probabilistic and deterministic full field approaches to simulate recrystallization in ods steels, Computational Materials Science 179 (2020) 109646. doi:10.1016/j.commatsci.2020.109646.

[19] D. Weygand, Y. Bréchet, J. Lépinoux, Zener pinning and grain growth: A two-dimensional vertex computer simulation, Acta Materialia 47 (3) (1999) 961–970. doi:10.1016/S1359-6454(98)00383-8.

[20] L. Vanherpe, N. Moelans, B. Blanpain, S. Vandewalle, Pinning effect of spheroid second-phase particles on grain growth studied by three-dimensional phase-field simulations, Computational Materials Science 49 (2) (2010) 340–350. doi:10.1016/j.commatsci.2010.05.020.

[21] K. Chang, W. Feng, L. Q. Chen, Effect of second-phase particle morphology on grain growth kinetics, Acta Materialia 57 (17) (2009) 5229–5236. doi:10.1016/j.actamat.2009.07.025.

[22] N. Moelans, B. Blanpain, P. Wollants, Pinning effect of second-phase particles on grain growth in polycrystalline films studied by 3-D phase field simulations, Acta Materialia 55 (6) (2007) 2173–2182. doi:10.1016/j.actamat.2006.11.018.

[23] K. Chang, J. Kwon, C. K. Rhee, Effect of particle-matrix coherency on Zener pinning: A phase-field approach, Computational Materials Science 142 (2018) 297–302. doi:10.1016/j.commatsci.2017.10.030.

[24] T. Chakrabarti, S. Manna, Zener pinning through coherent precipitate: A phase-field study, Computational Materials Science 154 (June) (2018) 84–90. doi:10.1016/j.commatsci.2018.07.041.

[25] M. Apel, B. Böttger, J. Rudnizki, P. Schaffnit, I. Steinbach, Grain Growth Simulations Including Particle Pinning Using the Multiphase-field Concept, ISIJ International 49 (7) (2009) 1024–1029. doi:10.2355/isijinternational.49.1024.

[26] C. Schwarze, R. Darvishi Kamachali, I. Steinbach, Phase-field study of zener drag and pinning of cylindrical particles in polycrystalline materials, Acta Materialia 106 (2016) 59–65. doi:10.1016/j.actamat.2015.10.045.

[27] R. Darvishi Kamachali, I. Steinbach, 3-D phase-field simulation of grain growth: Topological analysis versus mean-field approximations, Acta Materialia 60 (6-7) (2012) 2719–2728. doi:10.1016/j.actamat.2012.01.037.

[28] A. Agnoli, N. Bozzolo, R. Logé, J. M. Franchet, J. Laigo, M. Bernacki, Development of a level set methodology to simulate grain growth in the presence of real secondary phase particles and stored energy - Application to a nickel-base superalloy, Computational Materials Science 89 (2014) 233–241. doi:10.1016/j.commatsci.2014.03.054.

[29] B. Scholtes, D. Ilin, A. Settefrati, N. Bozzolo, A. Agnoli, M. Bernacki, Full field modeling of the Zener pinning phenomenon in a level set framework - Discussion of classical limiting mean grain size equation, Proceedings of the International Symposium on Superalloys 2016-Janua (2016) 497–503. doi:10.1002/9781119075646.ch53.

[30] B. Merriman, J. K. Bence, S. J. Osher, Motion of multiple junctions: A level set approach, Journal of Computational Physics (1994). doi:10.1006/jcph.1994.1105.

[31] M. Bernacki, H. Resk, T. Coupez, R. E. Logé, Finite element model of primary recrystallization in polycrystalline aggregates using a level set framework, Modelling and Simulation in Materials Science and Engineering 17 (6) (2009) 0–22. doi:10.1088/0965-0393/17/6/064006.

[32] M. Bernacki, R. E. Logé, T. Coupez, Level set framework for the finite-element modelling of recrystallization and grain growth in polycrystalline materials, Scripta Materialia 64 (6) (2011) 525–528. doi:10.1016/j.scriptamat.2010.11.032.

[33] D. N. Ilin, N. Bozzolo, T. Toulorge, M. Bernacki, Full field modeling of recrystallization: Effect of intragranular strain gradients on grain boundary shape and kinetics, Computational Materials Science 150 (2018) 149–161. doi:10.1016/j.commatsci.2018.03.063.

[34] S. Florez, M. Shakoor, T. Toulorge, M. Bernacki, A new finite element strategy to simulate microstructural evolutions, Computational Materials Science 172 (September 2019) (2020) 109335. doi:10.1016/j.commatsci.2019.109335.

[35] S. Osher, R. P. Fedkiw, Level Set Methods: An Overview and Some Recent Results, Journal of Computational Physics 169 (2) (2001) 463–502. doi:10.1006/jcph.2000.6636.

[36] J. Fausty, N. Bozzolo, D. P. Muoz], M. Bernacki, A novel level-set finite element formulation for grain growth with heterogeneous grain boundary energies, Materials & Design 160 (2018) 578 – 590. doi:10.1016/j.matdes.2018.09.050.

[37] J. Fausty, N. Bozzolo, M. Bernacki, A 2d level set finite element grain coarsening study with heterogeneous grain boundary energies, Applied Mathematical Modelling 78 (2020) 505 – 518. doi:10.1016/j.apm.2019.10.008.

[38] J. Furstoss, M. Bernacki, C. Petit, J. Fausty, D. PinoMuoz, C. Ganino, Full field and mean field modeling of grain growth in a multiphase material under dry conditions: Application to peridotites, Journal of Geophysical Research: Solid Earth 125 (1) (2020) e2019JB018138. doi:10.1029/2019JB018138.

[39] J. Fausty, N. Bozzolo, M. Bernacki, A 2d level set finite element grain coarsening study with heterogeneous grain boundary energies, Applied Mathematical Modelling 78 (2020) 505 – 518. doi:10.1016/j.apm.2019.10.008.

[40] J. Furstoss, M. Bernacki, C. Petit, J. Fausty, D. PinoMuoz, C. Ganino, Reconciliate laboratory and natural constraints for olivine grain growt kinetics: on the role of solute drag, Journal of Geophysical Research: Solid Earth Submitted.

[41] B. Scholtes, M. Shakoor, A. Settefrati, P. O. Bouchard, N. Bozzolo, M. Bernacki, New finite element developments for the full field modeling of microstructural evolutions using the level-set method, Computational Materials Science 109 (2015) 388–398. doi:10.1016/j.commatsci.2015.07.042.

[42] J. A. Sethian, A fast marching level set method for monotonically advancing fronts., Proceedings of the National Academy of Sciences 93 (4) (1996) 1591–1595. doi:10.1073/pnas.93.4.1591.

[43] J. A. Sethian, A. Vladimirsky, Fast methods for the Eikonal and related Hamilton- Jacobi equations on unstructured meshes, Proceedings of the National Academy of Sciences 97 (11) (2000) 5699–5703. doi:10.1073/pnas.090060097.

[44] M. Sussman, P. Smereka, S. Osher, A Level Set Approach for Computing Solutions to Incompressible Two-Phase Flow, Journal of Computational Physics 114 (1) (1994) 146–159. doi:10.1006/JCPH.1994.1155.

[45] M. Shakoor, B. Scholtes, P.-O. Bouchard, M. Bernacki, An efficient and parallel level set reinitialization method Application to micromechanics and microstructural evolutions, Applied Mathematical Modelling 39 (23-24) (2015) 7291–7302. doi:10.1016/j.apm.2015.03.014.

[46] T. Grosdidier, A. Hazotte, A. Simon, Precipitation and dissolution processes in γ/γ' single crystal nickel-based superalloys, Materials Science and Engineering A 256 (1-2) (1998) 183–196. doi:10.1016/s0921-5093(98)00795-3.

[47] F. Masoumi, M. Jahazi, D. Shahriari, J. Cormier, Coarsening and dissolution of γ' precipitates during solution treatment of AD730 Ni-based superalloy: Mechanisms and kinetics models, Journal of Alloys and Compounds 658 (2016) 981–995. doi:10.1016/j.jallcom.2015.11.002.

[48] M. Bernacki, Y. Chastel, T. Coupez, R. Log, Level set framework for the numerical modelling of

primary recrystallization in polycrystalline materials, Scripta Materialia 58 (12) (2008) 1129 – 1132. doi:10.1016/j.scriptamat.2008.02.016.

[49] A. Cruz-Fabiano, R. Log, M. Bernacki, Assessment of simplified 2d grain growth models from numerical experiments based on a level set framework, Computational Materials Science 92 (2014) 305 – 312. doi:10.1016/j.commatsci.2014.05.060.

[50] Y. Jin, N. Bozzolo, A. Rollett, M. Bernacki, 2d finite element modeling of misorientation dependent anisotropic grain growth in polycrystalline materials: Level set versus multi-phase-field method, Computational Materials Science 104 (2015) 108 – 123. doi:10.1016/j.commatsci.2015.03.012.

[51] K. Hitti, P. Laure, T. Coupez, L. Silva, M. Bernacki, Precise generation of complex statistical representative volume elements (rves) in a finite element context, Computational Materials Science 61 (2012) 224 – 238. doi:10.1016/j.commatsci.2012.04.011.

[52] B. Scholtes, M. Shakoor, N. Bozzolo, P.-O. Bouchard, A. Settefrati, M. Bernacki, Advances in level-set modeling of recrystallization at the polycrystal scale - development of the digi-μ software, Key Engineering Materials 651–653 (2015) 617–623. doi:10.4028/www.scientific.net/KEM.651-653.617.